Cellular and Molecular Life Sciences (2023) 80:213
https://doi.org/10.1007/s00018-023-04863-z

ORIGINAL ARTICLE

DUSP1 interacts with and dephosphorylates VCP to improve mitochondrial quality control against endotoxemia-induced myocardial dysfunction

Hang Zhu[1] · Jin Wang[2] · Ting Xin[3] · Shanshan Chen[1] · Ruiying Hu[1] · Yukun Li[4] · Mingming Zhang[5] · Hao Zhou[1]

Received: 22 May 2023 / Revised: 1 July 2023 / Accepted: 7 July 2023 / Published online: 18 July 2023

Abstract

Dual specificity phosphatase 1 (DUSP1) and valosin-containing protein (VCP) have both been reported to regulate mitochondrial homeostasis. However, their impact on mitochondrial quality control (MQC) and myocardial function during LPS-induced endotoxemia remains unclear. We addressed this issue by modeling LPS-induced endotoxemia in DUSP1 transgenic ($DUSP1^{TG}$) mice and in cultured DUSP1-overexpressing HL-1 cardiomyocytes. Accompanying characteristic structural and functional deficits, cardiac DUSP1 expression was significantly downregulated following endotoxemia induction in wild type mice. In contrast, markedly reduced myocardial inflammation, cardiomyocyte apoptosis, cardiac structural disorder, cardiac injury marker levels, and normalized systolic/diastolic function were observed in $DUSP1^{TG}$ mice. Furthermore, DUSP1 overexpression in HL-1 cells significantly attenuated LPS-mediated mitochondrial dysfunction by preserving MQC, as indicated by normalized mitochondrial dynamics, improved mitophagy, enhanced biogenesis, and attenuated mitochondrial unfolded protein response. Molecular assays showed that VCP was a substrate of DUSP1 and the interaction between DUSP1 and VCP primarily occurred on the mitochondria. Mechanistically, DUSP1 phosphatase domain promoted the physiological DUSP1/VCP interaction which prevented LPS-mediated VCP Ser784 phosphorylation. Accordingly, transfection with a phosphomimetic VCP mutant abolished the protective actions of DUSP1 on MQC and aggravated inflammation, apoptosis, and contractility/relaxation capacity in HL-1 cardiomyocytes. These findings support the involvement of the novel DUSP1/VCP/MQC pathway in the pathogenesis of endotoxemia-caused myocardial dysfunction.

Keywords Endotoxemia-caused myocardial dysfunction · DUSP1 · VCP · Mitochondrial quality control · Mitochondria · Myocardial inflammation · Apoptosis · Oxidative stress

Hang Zhu and Jin Wang contributed equally to this article.

✉ Mingming Zhang
winterzhang3@163.com

✉ Hao Zhou
zhouhao@plagh.org

1 Senior Department of Cardiology, The Sixth Medical Center of People's Liberation Army General Hospital, Beijing 100048, China

2 Department of Vascular Medicine, Peking University Shougang Hospital, Beijing 100144, China

3 Department of Cardiology, Tianjin First Central Hospital, 24 Fukang Road, Nankai District, Tianjin 300192, People's Republic of China

4 Department of Cardiology, Beijing Anzhen Hospital, Capital Medical University, Beijing 100029, China

5 Department of Cardiology, Tangdu Hospital, Air Force Medical University, Xi'an 710038, China

Introduction

Sepsis is a systemic condition caused by an abnormal host response to infection. Endotoxemia-caused myocardial dysfunction is a frequent complication of sepsis, characterized by acutely depressed left ventricular ejection fraction (LVEF) with ventricular dilation [1]. Although most patients with myocardial dysfunction induced by endotoxemia recover within 7–10 days, endotoxemia-related mortality remains high [2]. Several pathophysiological factors have been proposed to explain the etiology of endotoxemia-caused myocardial dysfunction. These include oxidative stress, an abnormal inflammatory response, complement system activation, intracellular calcium overload, reduced microvascular perfusion, fibrin deposition, and tissue hypoxia [3, 4]. Accumulating evidence highlights the important role played by mitochondrial dysfunction in endotoxemia-caused

myocardial dysfunction. Abnormal mitochondrial fission [5], defective mitochondrial metabolism [6], and increased mitochondrial reactive oxygen species (ROS) production [7] are closely associated with heart failure during endotoxemia. In addition, dysregulated mitochondrial calcium handling [8] and mitochondria-dependent apoptosis [9] were also reported to contribute to endotoxemia-related cardiomyocyte damage and dysfunction. In response to mitochondrial damage, two intrinsic repairing mechanisms are typically activated: the mitochondrial unfolded protein response (UPR^{mt}), which acts to restore mitochondrial proteostasis, and the mitochondrial quality control (MQC) system, which serves to preserve mitochondrial dynamics through regulating fission and fusion events, mitophagy, and mitochondrial biogenesis. Our previous study described the molecular basis of altered UPR^{mt} in the progression of endotoxemia-related myocardial dysfunction [10]. However, little is known about the precise role and regulatory mechanism of MQC in endotoxemia-caused cardiac depression.

Dual specificity phosphatase 1 (DUSP1) is a phosphatase with dual specificity for tyrosine and threonine. It is able to recognize phospho-Ser/Thr and phospho-Tyr residues in substrates [11]. It was originally discovered as an upstream regulator of mitogen-activated protein kinase (MAPK) via dephosphorylation of MAPK/extracellular regulated protein kinases (ERK), MAPK/c-Jun N-terminal kinase (JNK), and MAPK/p38 [12, 13]. Our recent study demonstrated a protective role of DUSP1, mediated by inhibition of mitochondrial fission and mitophagy activation, in the context of cardiac ischemia/reperfusion (I/R) injury [14]. In line with these findings, several reports further confirmed the beneficial effects offered by DUPS1 on mitochondrial homeostasis. Thus, DUSP1 expression was shown to reduce mitochondria-related oxidative stress injury in sensorineural hearing loss [15], repress mitochondrial fission in diabetic nephropathy [16], restore PARKIN-related mitophagy in the post-ischemic myocardium [17], inhibit neuroinflammation-related, mitochondria-initiated apoptosis [18], and improve mitochondrial metabolism in obesity [19]. Adding to this evidence suggestive of a central role for DUSP1 in maintaining MQC, numerous studies highlighted the anti-inflammatory properties of DUSP1 in endotoxemia-related organ dysfunction [20–24]. Hence, we hypothesized that DUSP1 activity might attenuate endotoxemia-caused myocardial dysfunction through improving MCQ and counteracting the inflammatory response.

Valosin-containing protein (VCP), a member of the AAA class of ATPases, is highly conserved from archaebacteria to humans and is mainly located in subcellular organelles such as the endoplasmic reticulum (ER), mitochondria, and nucleus. The primary function of VCP is to assist protein degradation by the proteasome. Gain-of-function mutations in VCP have been reported to cause a hereditary multisystem disease known as inclusion body myopathy associated with Paget's disease of bone and frontotemporal dementia (IBMPFD) [25]. Molecular studies on inclusion body myopathy with early-onset Paget disease and frontotemporal dementia (IBMPFD) pathogenesis revealed reduced ATP levels, depressed reserve respiratory capacity, and increased proton leak and glycolysis in IBMPFD patient-derived myoblasts/fibroblasts [26]. A role for VCP in cardiovascular disease was suggested by a study showing that selective inhibition of VCP through administration of KUS121 was able to reduce cardiac damage in murine and porcine models of myocardial infarction [27]. Meanwhile, a study reported that VCP recruitment to mitochondria induces excessive mitophagy and promotes neurodegeneration in Huntington's disease models [28]. Interestingly, aggregation of VCP at perinuclear regions was shown to promote survival of serum-starved prostate cancer cells by lowering the cells' metabolic rate through decreasing mitochondrial activity [29]. Importantly, VCP was shown to play an essential role in the regulation of MQC through interactions with the PINK1/PARKIN pathway [30]. Recent evidence revealed that VCP phosphorylation at Ser784 is promoted by the DNA damage response and enhances VCP function in various diseases, such as *H. pylori*-induced gastritis and breast cancer [31–33]. However, it remains unknown whether VCP phosphorylation contributes to the progression of endotoxemia-caused myocardial dysfunction through disrupting MQC.

Considering the protective role of DUSP1 against sepsis-related organ dysfunction through its phosphatase activity, in this study we asked whether DUSP1 is able to reduce or prevent VCP phosphorylation to normalize MQC and alleviate heart dysfunction caused by endotoxemia.

Results

DUSP1 overexpression alleviates LPS-mediated myocardial inflammation and cardiomyocyte death

To analyze potential alterations in DUSP1 expression in the course of endotoxemia, Western blot analysis was performed in mouse heart lysates after LPS-induced endotoxemia. Cardiac expression of DUSP1 was significantly downregulated in LPS-treated compared to control mice (Fig. 1A and B). To investigate the role of DUSP1 in endotoxemia, DUSP1 transgenic ($DUSP1^{TG}$) mice were injected with LPS and immunofluorescence assays were used to assess myocardial inflammation. As shown in Fig. 1C and D, compared with the control group, extensive $GR1^+$ immunoreactivity indicated marked neutrophil infiltration in heart tissues from wild type (WT) mice treated with LPS. In contrast, no significant change in $GR1^+$ neutrophil numbers was observed

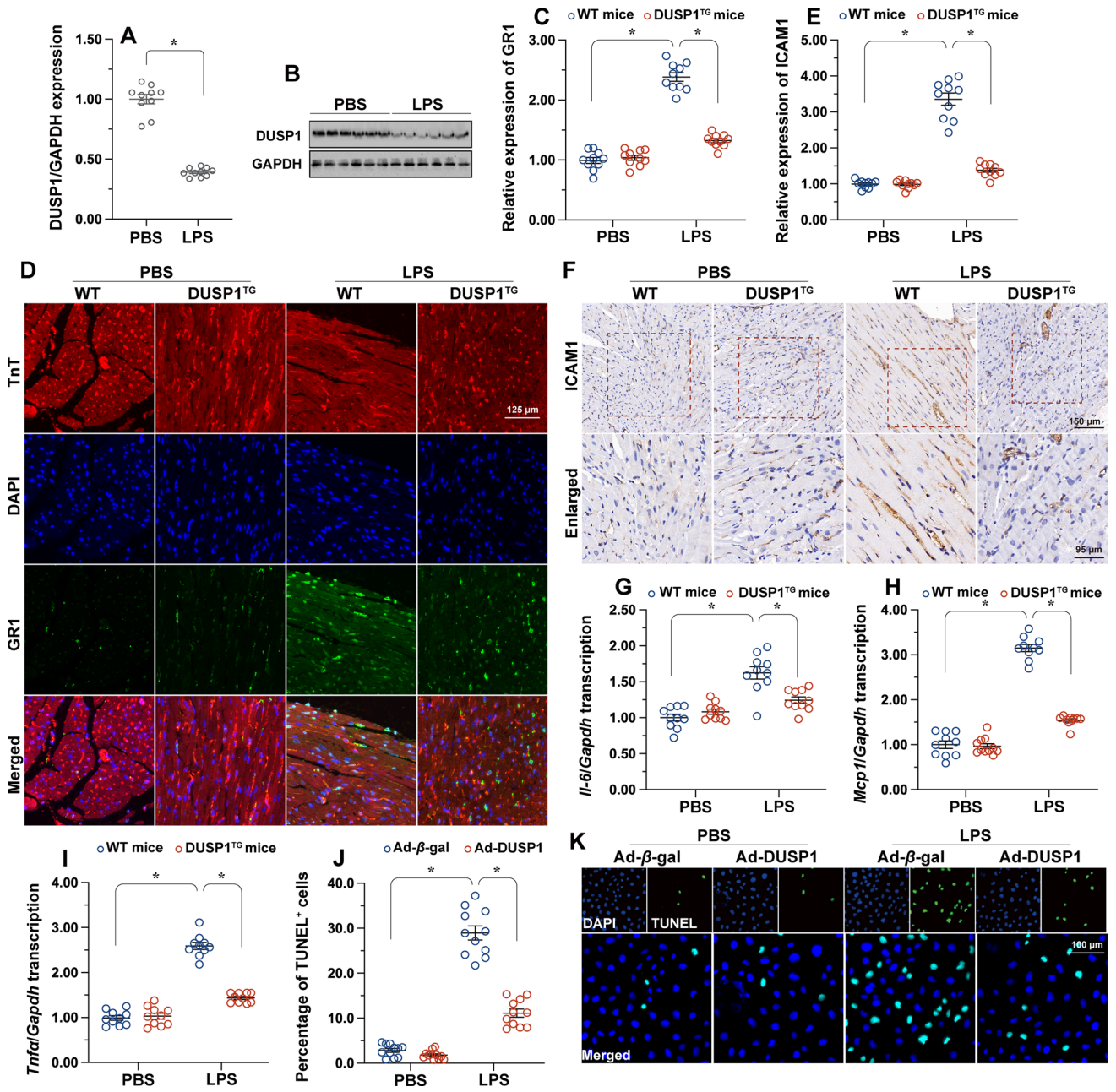

Fig. 1 DUSP1 overexpression alleviates LPS-induced myocardial inflammation and cardiomyocyte death. **A**, **B** Western blot analysis of DUSP1 expression in heart extracts from control and LPS-treated mice. GAPDH was used as internal control for normalization. Scale bar, 125 μm. **C**, **D** Representative GR1 immunofluorescence images and quantification of Gr-1^{+} neutrophils in heart tissues. **E**, **F** Representative images of ICAM1 immunohistochemistry in heart tissues and corresponding quantification data. Scale bar, 150 μm. **G**–**I** Relative expression of *Il-6*, *Mcp1*, and *Tnfα* in cardiac tissue determined via qPCR. *Gapdh* was used as internal control to normalize expression data. **J**, **K** Representative images of TUNEL staining in HL-1 cells and quantification of TUNEL-positive cells. Scale bar, 100 μm. Data are shown as mean ± SEM ($n = 10$ mice per group). *$p < 0.05$

in cardiac samples from LPS-treated DUSP1^{TG} mice. Consistent with these findings, immunohistochemistry results showed that after treatment with LPS the expression of ICAM1 (a cell adhesion factor) was increased in heart tissue from WT mice, while this change was virtually undetectable in heart samples from DUSP1^{TG} mice (Fig. 1E and F). Moreover, qPCR assays indicated that the transcription of pro-inflammation cytokines, namely *Il-6*, *Mcp1*, and *Tnfα*, was significantly increased in response to LPS treatment in WT mice. However, this pro-inflammatory phenotype was not evident in cardiac tissue from DUSP1^{TG} mice (Fig. 1G–I).

In addition to myocardial inflammation, cardiomyocyte death has been regarded as a potential mechanism contributing to depressed cardiac function during endotoxemia. TUNEL staining demonstrated that relative to control mice, LPS-treated WT mice showed extensive apoptosis of cardiomyocytes (Supporting Fig. S1A, B). Consistently, compared to control tissues, the activity of caspase-3, a marker of cellular apoptosis, was relatively increased in heart samples from LPS-treated mice (Supporting Fig. S1C). However, no significant changes in TUNEL labeling (Supporting Fig. S1A, B) and caspase-3 activity (Supporting Fig. S1C) were detected in hearts from DUSP1^{TG} mice.

To further verify the cardioprotective actions of DUSP1, we used cultured HL-1 cells challenged with LPS as an in vitro model of endotoxemia. DUSP1 overexpression was induced through adenovirus-mediated gene transfer (Ad-DUSP1), and Ad-β-gal-transduced cells were used as a control group. LPS treatment upregulated the transcription of pro-inflammatory factors in Ad-β-gal-transduced, but not in Ad-DUSP1-transduced, cardiomyocytes (Supporting Fig. S1D-F). In turn, TUNEL positivity was increased after LPS exposure in control but not in DUSP1-overexpressing cardiomyocytes (Fig. 1J and K). These results indicate that DUSP1 overexpression reduces the cardiac inflammatory response and prevents cardiomyocyte death mediated by LPS.

DUSP1 overexpression reduces endotoxemia-induced myocardial structural disorder

Next, we used electron microscopy (TEM) to assess whether DUSP1 overexpression preserves myocardial ultrastructure during LPS-induced endotoxemia. Displaced myofibrils with tortuous, mismatched Z discs were noted in the myocardium of LPS-treated WT mice (Fig. 2A, white arrows). In addition, most cardiomyocytes in these samples showed disorganized mitochondria with disrupted contact sites, while some mitochondria presented also as large vacuoles, formed upon complete cristae destruction and "watering" of the matrix (Fig. 2A, yellow arrows). However, these structural alterations were largely absent in the hearts of LPS-treated DUSP1^{TG} mice (Fig. 2A). In line with these findings, HE staining results also showed disarranged myofibrils in LPS-treated WT mice, and marked preservation of cardiac myofibrils in LPS-treated DUSP1^{TG} mice (Fig. 2B). Consistent with these changes, serum troponin T (TnT), CK-MB, and LDH levels were significantly upregulated in LPS-treated WT mice (Fig. 2C–E). However, overexpression of DUSP1 prevented the upregulation of the above cardiac injury markers in response to LPS (Fig. 2C–E).

Next, myosin immunofluorescence was conducted in HL-1 cells to assess the impact of DUSP1 overexpression on cardiomyocyte structure after exposure to LPS. Results showed obvious disruption of myosin filaments in LPS-treated control cells (Fig. 2F and G). Additionally, the expression of myosin was slightly downregulated in these cells (Fig. 2F and G). Interestingly, transfection with Ad-DUSP1 normalized the expression and organization of myosin (Fig. 2F and G). We next used ELISA to evaluate the release of cardiac injury markers by HL-1 cells. Cell culture supernatant levels of TnT, CK-MB, and LDH were markedly increased by LPS exposure in Ad-β-gal-transduced but not Ad-DUSP1-transduced cardiomyocytes (Fig. 2H–J). These results confirmed that LPS-induced myocardial structural alterations can be attenuated by DUSP1 overexpression.

DUSP1 overexpression prevents endotoxemia-induced cardiac dysfunction

Cardiac dysfunction, especially decreased LVEF, has been regarded as a diagnostic standard for endotoxemia-caused myocardial dysfunction. Accordingly, echocardiography was used to analyze changes in cardiac function upon LPS treatment. As shown in Table 1, cardiac systolic indicators, including LVEF, ratio of left ventricular fractional shortening, and left ventricular systolic dimension, were altered in WT mice treated with LPS (Table 1). In turn, ratio of early to late transmitral flow velocities and left ventricular diastolic dimension, the diastolic function parameter, were markedly elevated in these mice (Table 1). Moreover, reduction in interventricular septum (IVS) thickness was also noted in LPS-treated WT mice (Table 1). However, improved systolic/diastolic capacity and normalized cardiac function parameters were recorded in DUSP1^{TG} mice (Table 1).

We next analyzed the contractile capacities of single, freshly isolated cardiomyocytes from WT or DUSP1^{TG} mice. Neither LPS stress nor DUSP1 overexpression influenced resting cardiomyocyte length (Fig. 3A). However, suppressed contractile capacity, evidenced by decreased peak shortening (PS), maximal velocity of shortening (+dL/dt), and time-to-peak shortening (TPS), was apparent following exposure to LPS (Fig. 3B–D). Similarly, cardiomyocyte relaxation parameters, including maximal velocity of relengthening (− dL/dt) and time-to-90% relengthening (TR90), were also impaired by LPS (Fig. 3E, F). Of note, LPS failed to perturb single cardiomyocyte contractile/relaxation capacities in DUSP1-overexpressing cells (Fig. 3A–F). These findings indicate that DUSP1 activity protects cardiomyocyte function and preserves myocardial performance in the setting of LPS-induced endotoxemia.

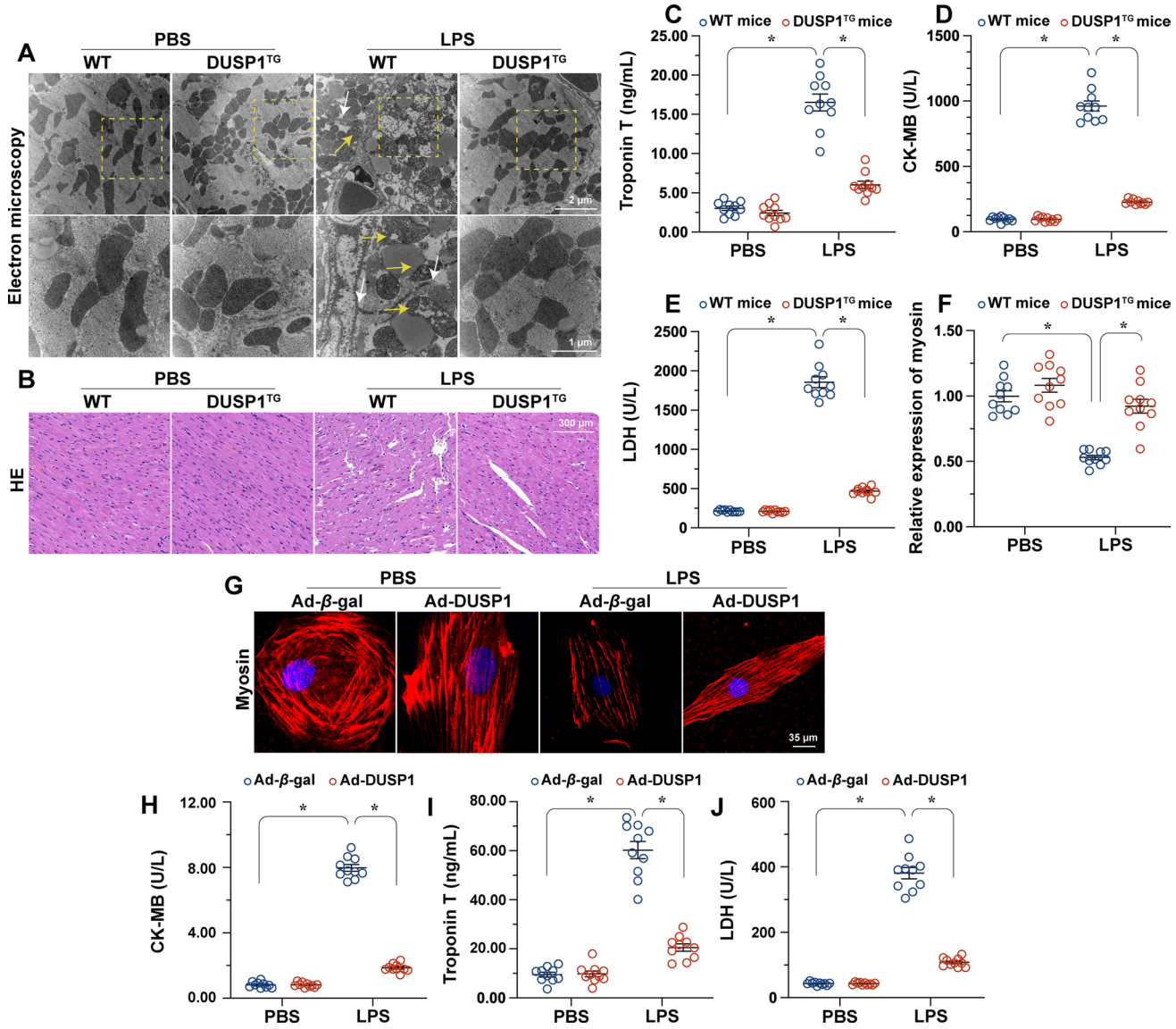

Fig. 2 DUSP1 overexpression reduces LPS-mediated myocardial structural disorder. **A** Representative TEM images of heart tissues from control and LPS-treated mice. White arrows indicate disorganized myofibrils and tortuous Z discs while yellow arrows indicate swollen mitochondria. Scale bar, 2 μm. **B** Representative HE images of heart tissues after endotoxemia induction. Scale bar, 300 μm. **C**–**E** Serum TnT, CK-MB, and LDH levels were determined by ELISA. **F**, **G** Representative myosin immunofluorescence images of cardiomyocytes exposed to LPS. Myosin expression levels were normalized to those of the control group. Scale bar, 35 μm. **H**–**J** TnT, CK-MB, and LDH levels in cell culture supernatants were determined by ELISA. Data are shown as mean ± SEM ($n = 10$ mice per group or ten independent cell isolations per group). *$p < 0.05$

DUSP1 overexpression prevents LPS-mediated mitochondrial dysfunction

Mitochondrial dysfunction is considered a key inducer of myocardial inflammation, structural disorder, and dysfunction during hypoxic and septic insults. We thus asked whether DUSP1-mediated cardioprotection during endotoxemia is attributable to improved mitochondrial function. ELISA results showed that LPS treatment reduced ATP production in Ad-β-gal-transduced but not in Ad-DUSP1-transduced HL-1 cardiomyocytes (Fig. 4A). In light of the indispensable role played by the mitochondrial membrane potential (MMP) in ATP production, changes in MMP were recorded in HL-1 cells loaded with the JC-1 probe. After exposure to LPS, MMP was reduced in Ad-β-gal-transduced cardiomyocytes (Fig. 4B and C). This change was undetectable, however, in DUSP1-overexpressing cells (Fig. 4B and C). Moreover, the production of mitochondrial ROS, assessed with MitoSOX Red, was significantly increased by LPS, and DUSP1 overexpression nullified this

Table 1 Echocardiographic analysis of systolic (LVEF, FS, and LVDs) and diastolic (LVDd, E/A) function and structural myocardial parameters (IVS and PW thickness) in mice treated with LPS

Parameter	PBS		LPS	
	WT mice	DUSP1^{TG} mice	WT mice	DUSP1^{TG} mice
BW, g	26.1 ± 0.9	26.1 ± 1.0	25.9 ± 1.1	26.0 ± 0.9
HW, mg	156.4 ± 7.9	155.6 ± 8.7	232.6 ± 7.1$^{\#}$	184.7 ± 9.1*
HW/BW, mg/g	5.91 ± 0.28	5.99 ± 0.31	7.88 ± 0.34$^{\#}$	6.42 ± 0.41*
LVDd, mm	3.25 ± 0.14	3.30 ± 0.12	3.95 ± 0.16$^{\#}$	3.56 ± 0.13*
LVDs, mm	2.23 ± 0.08	2.30 ± 0.09	3.24 ± 0.19$^{\#}$	2.53 ± 0.11*
IVS, mm	0.81 ± 0.03	0.82 ± 0.03	0.69 ± 0.04$^{\#}$	0.78 ± 0.04*
PW, mm	0.77 ± 0.05	0.76 ± 0.04	0.73 ± 0.02	0.77 ± 0.03
FS, %	33.8 ± 1.8	33.9 ± 2.1	21.3 ± 2.4$^{\#}$	29.8 ± 2.1*
EF, %	62.1 ± 2.5	62.3 ± 2.7	43.5 ± 5.4$^{\#}$	57.9 ± 4.5*
E/A	1.29 ± 0.21	1.32 ± 0.17	0.84 ± 0.09$^{\#}$	1.12 ± 0.16*

Data are shown as means ± standard error of the mean (SEM)

BW body weight; HW, heart weight; *LVDd* diastolic dimension of left ventricle; *LVDs* systolic dimension of left ventricle; *IVS* thickness of interventricular septum; *PW* thickness of posterior wall; *E/A* ratio of early to late transmitral flow velocities; *FS* ratio of left ventricular fractional shortening

$^{\#}p < 0.05$ vs. PBS + WT mice, $^{*}p < 0.05$ vs. PBS + DUSP1^{TG} mice

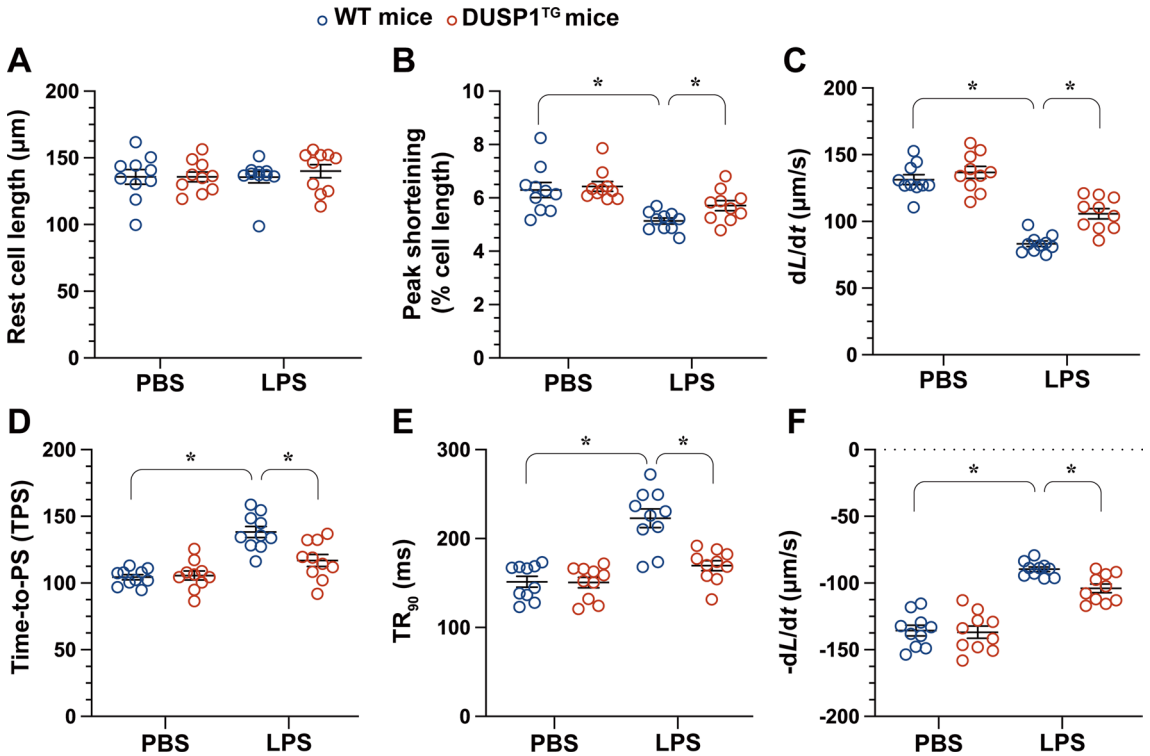

Fig. 3 DUSP1 overexpression prevents LPS-induced cardiac dysfunction. **A**–**F** Analysis of contractility/relaxation properties in acutely isolated adult mouse cardiomyocytes. Cardiomyocyte length, peak shortening (PS), maximal velocity of shortening (+dL/dt), time-to-peak shortening (TPS), the maximal velocity of relengthening (− dL/dt) and time-to-90% relengthening (TR90) were recorded. Data are shown as mean ± SEM (n = ten independent cell isolations per group). $^{*}p < 0.05$

effect (Fig. 4D and E). To investigate the mechanism underlying LPS-mediated MMP depolarization, we measured mitochondrial permeability transition pore (mPTP) opening. As shown in Fig. 4F, LPS extended the opening time of the mPTP in Ad-β-gal-transduced, but not in DUSP1-overexpressing, cardiomyocytes. Mitochondrial oxygen consumption rate (OCR) results further demonstrated that LPS treatment markedly reduced mitochondrial respiration

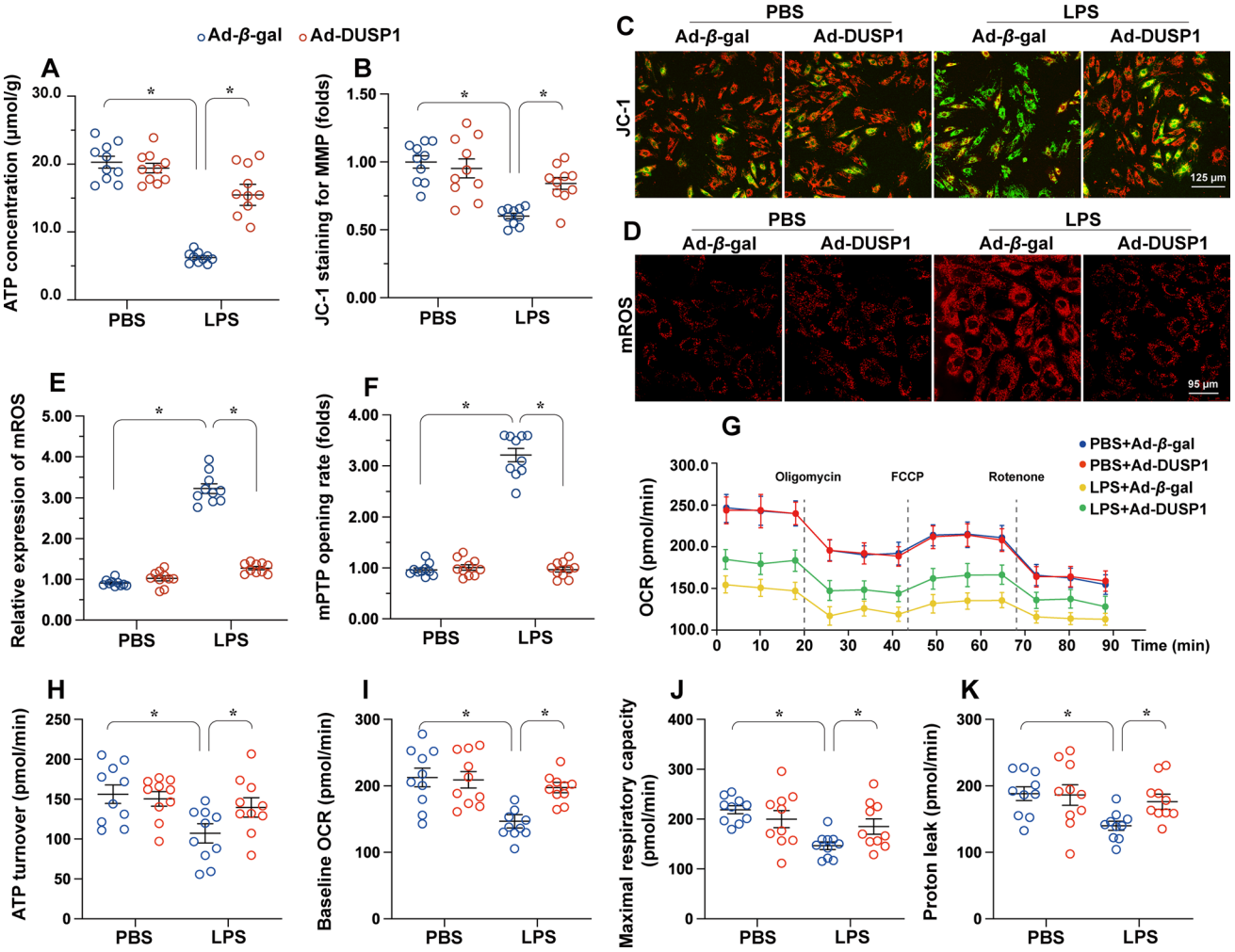

Fig. 4 DUSP1 supports mitochondrial function during LPS exposure. **A** ELISA analysis of total ATP production in cultured HL-1 cardiomyocytes. **B**, **C** Representative images of mitochondrial membrane potential (MMP) detection in cardiomyocytes loaded with the JC-1 probe and corresponding quantification data. Scale bar, 125 μm. **D**, **E** Representative images of mitochondrial ROS (mROS) detection in HL-1 cells loaded with the superoxide indicator MitoSOX Red. Scale bar, 95 μm. **F** Analysis of mPTP opening rate in HL-1 cells loaded with tetramethylrhodamine ethyl ester. **G**–**K** Mitochondrial oxygen consumption rate (OCR) was determined by the Seahorse XF real-time ATP rate assay using an XF-24 Extracellular Flux Analyzer. ATP turnover, baseline OCR, maximal respiration capacity and proton leak were measured in HL-1 cells treated with Ad-β-gal or Ad-DUSP1. Data are shown as mean ± SEM (n = ten independent cell isolations per group). *$p < 0.05$

in control but not in DUSP1-overexpressing cardiomyocytes (Fig. 4G–K). These data indicate that DUSP1 sustains mitochondrial function during LPS stress.

Mitochondrial quality control is normalized by DUSP1

Mitochondrial dysfunction can be attenuated or prevented by activation of the MQC system, which regulates mitochondrial fission/fusion cycles and biogenesis, as well as mitophagy. Considering the protective impact of DUSP1 on mitochondrial homeostasis, we questioned whether MQC activation was induced by DUSP1 to maintain mitochondrial function. Western blot analysis in heart lysates showed that LPS upregulated the expression fission-related proteins (DRP1 and FIS1) and inhibited the expression of fusion-related proteins (MFN2/OPA1) (Fig. 5A–E). Consistent with these results, in vitro exposure of HL-1 cells to LPS promoted the formation of round, small, fragmented mitochondria, suggesting increased fission and decreased fusion (Fig. 5F–H). However, overexpression of DUSP1 restored the balance of fission and fusion markers both in the heart (Fig. 5A–E) and in HL-1 cells in vitro (Fig. 5F–H).

Additional western blot assays showed that cardiac expression of the mitophagy-related proteins ATG5, BECLIN1, and PARKIN was downregulated by LPS treatment

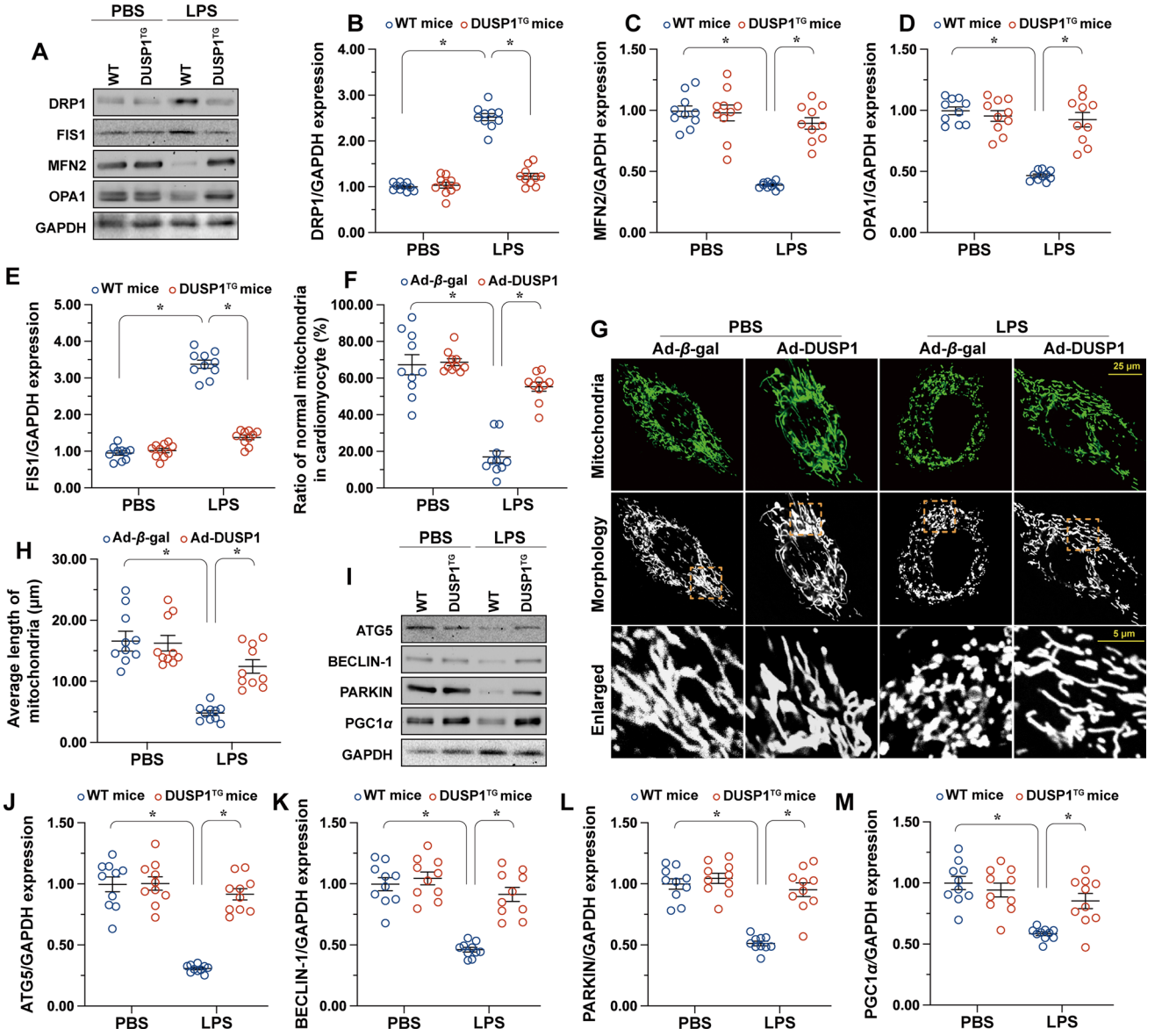

Fig. 5 DUSP1 overexpression normalizes mitochondrial fission and mitophagy during endotoxemia-caused myocardial depression. **A**–**E**. Western blot analysis of DRP1, FIS1, MFN2, and OPA1 expression in heart extracts. GAPDH was used as internal control. **F**–**H** Representative images of Tom-20 immunofluorescence in cardiomyocytes illustrating mitochondrial morphology in the absence and presence of LPS and quantification of average mitochondrial length and percentage of cardiomyocytes with fragmented mitochondria. Scale bar, 25 μm. **I**–**M** Western blots analysis of ATG5, BECLIN1, PARKIN, and PGC-1α expression in heart lysates. GAPDH was used as internal control. Data are shown as mean ± SEM ($n = 10$ mice per group or ten independent cell isolations per group). *$p < 0.05$

(Fig. 5I–M), suggestive of defective mitophagy. In line with these data, in vitro assessment of mitophagy in HL-1 cells expressing the fluorescent mt-Keima reporter showed that mitophagic activity was significantly impaired by LPS (Fig. 6A and B). Interestingly, DUSP1 overexpression not only prevented the downregulation of mitophagy-related proteins (Supporting Fig. S2A–E), but also rescued mitophagic activity in cultured HL-1 cardiomyocytes (Supporting Fig. S2A–E).

Notably, the accumulation of mitophagy-related proteins may be derived from mitophagy induction or the interruption of autophagic flux. To rule out the latter, Bafilomycin-A1 (Baf-A1) was employed. In DUSP1-overexpressed cells, Baf-A1 further upregulated mito-LC3II and LC3II expressions but disrupted p62 degradation (Supporting Fig. S2A-E). Moreover, the levels of TIM23 (mitochondrial inner membrane marker) and TOM20 (outer membrane marker) were significantly elevated upon LPS treatment and was

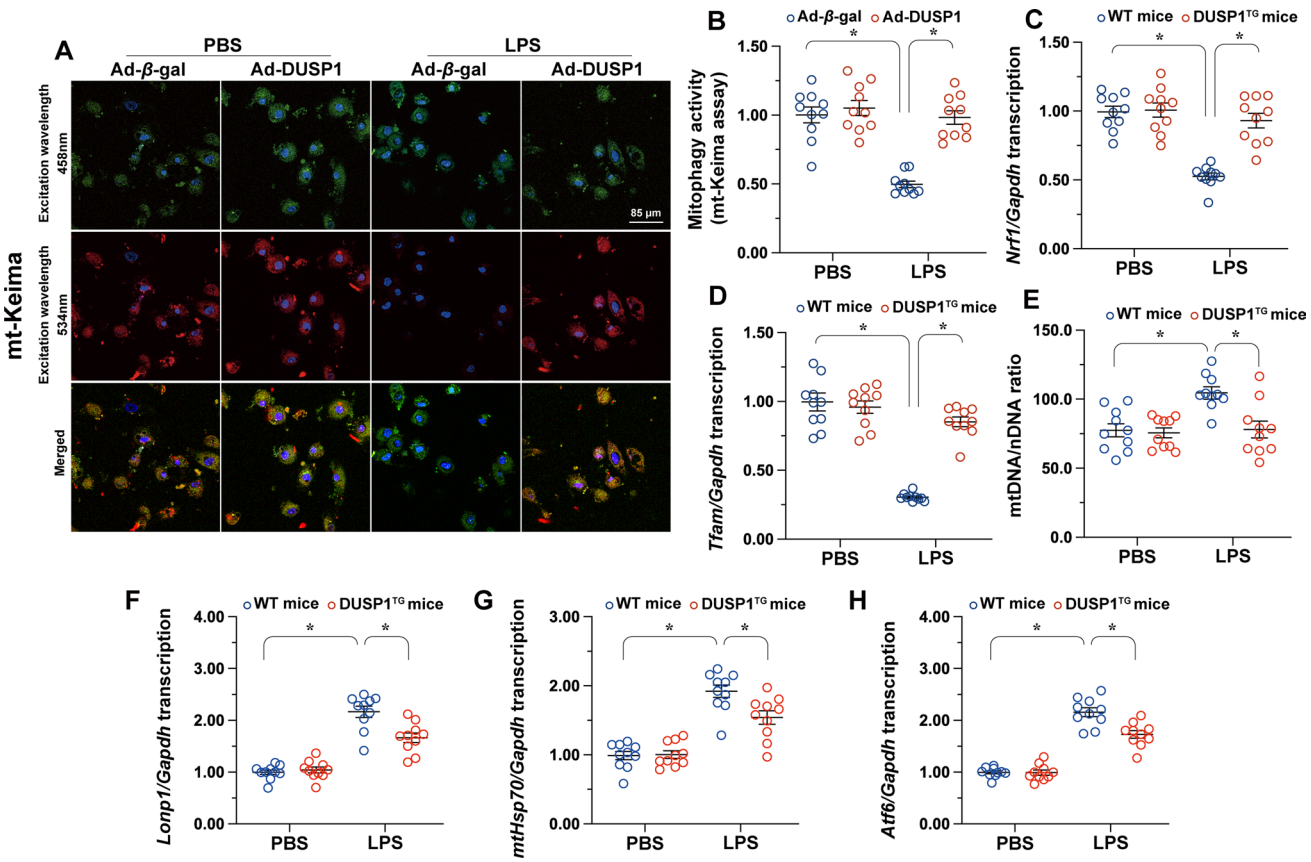

Fig. 6 Overexpression of DUSP1 reverses mitophagy, mitochondrial biogenesis and mitochondrial unfolded protein response during endotoxemia-caused myocardial depression. **A**, **B** Detection and quantification of mitophagic activity in cardiomyocytes expressing the mt-Keima reporter. Scale bar, 85 μm. **C**, **D** Relative *Nrf1* and *Tfam* expression levels were determined via qPCR. GAPDH was used as internal control. **E** The *Co1* gene of the mtDNA and the *Ndufv1* nDNA gene were amplified by qPCR to determine the relative mtDNA/nDNA ratio. **F**–**H** Relative *Lonp1*, *mtHsp70*, *Atf6* expression levels were determined via qPCR. GAPDH was used as internal control. Data are shown as mean ± SEM ($n = 10$ mice per group or ten independent cell isolations per group). *$p < 0.05$

reduced in response to DUSP1 overexpression. Supplementation of Baf-A1 promoted the accumulation of TIM23 and TOM20 in DUSP1-overexpressed cells (Supporting Fig. S2A-E). Overall, mitophagy is inhibited by LPS and was restored by DUSP1 overexpression.

Mitochondrial biogenesis is primarily regulated by PGC-1α and its downstream transcription factors *Nrf1* and *Tfam*1. We noted that LPS treatment reduced PGC-1α protein expression (Fig. 5I and M) and transcriptional levels of *Nrf1*/*Tfam1* in heart tissue from WT mice but not from DUSP1^{TG} mice (Fig. 6C and D). To understand the net effects of altered mitophagy and abnormal biogenesis on mitochondrial mass, the ratio of mtDNA/nDNA were determined. LPS significantly elevated the ratio of mtDNA/nDNA in the heart tissues from WT mice while this result was reversed in DUSP1^{TG} mice (Fig. 6E).

Lastly, mitochondrial unfolded protein response (UPR^{mt}) has been identified as a regulator of MQC. In our study, the parameters related to UPR^{mt} were slightly increased at the transcriptional levels in answer to LPS treatment (Fig. 6F–H), suggesting an activation of mitochondrial stress response. However, DUSP1 overexpression suppressed the levels of UPR^{mt}-related markers (Fig. 6F–H). In sum, these data suggest that MQC function is impaired during endotoxemia-caused myocardial dysfunction and that this effect can be largely prevented by DUSP1 overexpression.

DUSP1 binds to VCP and prevents endotoxemia-mediated VCP phosphorylation

Recent evidence identified VCP as a novel regulator of MQC via induction of proteasome-mediated protein degradation [27], an effect promoted by VCP phosphorylation [31–33]. Thus, we asked whether an altered VCP phosphorylation status might mediate LPS-induced MQC impairment. Western blot assays in cardiac tissue demonstrated that total VCP level was not affected by LPS. However, VCP phosphorylation at Ser784 was upregulated by LPS and downregulated by DUSP1 overexpression (Fig. 7A–C). These data led us to speculate that the protective effect of DUSP1 on cardiac

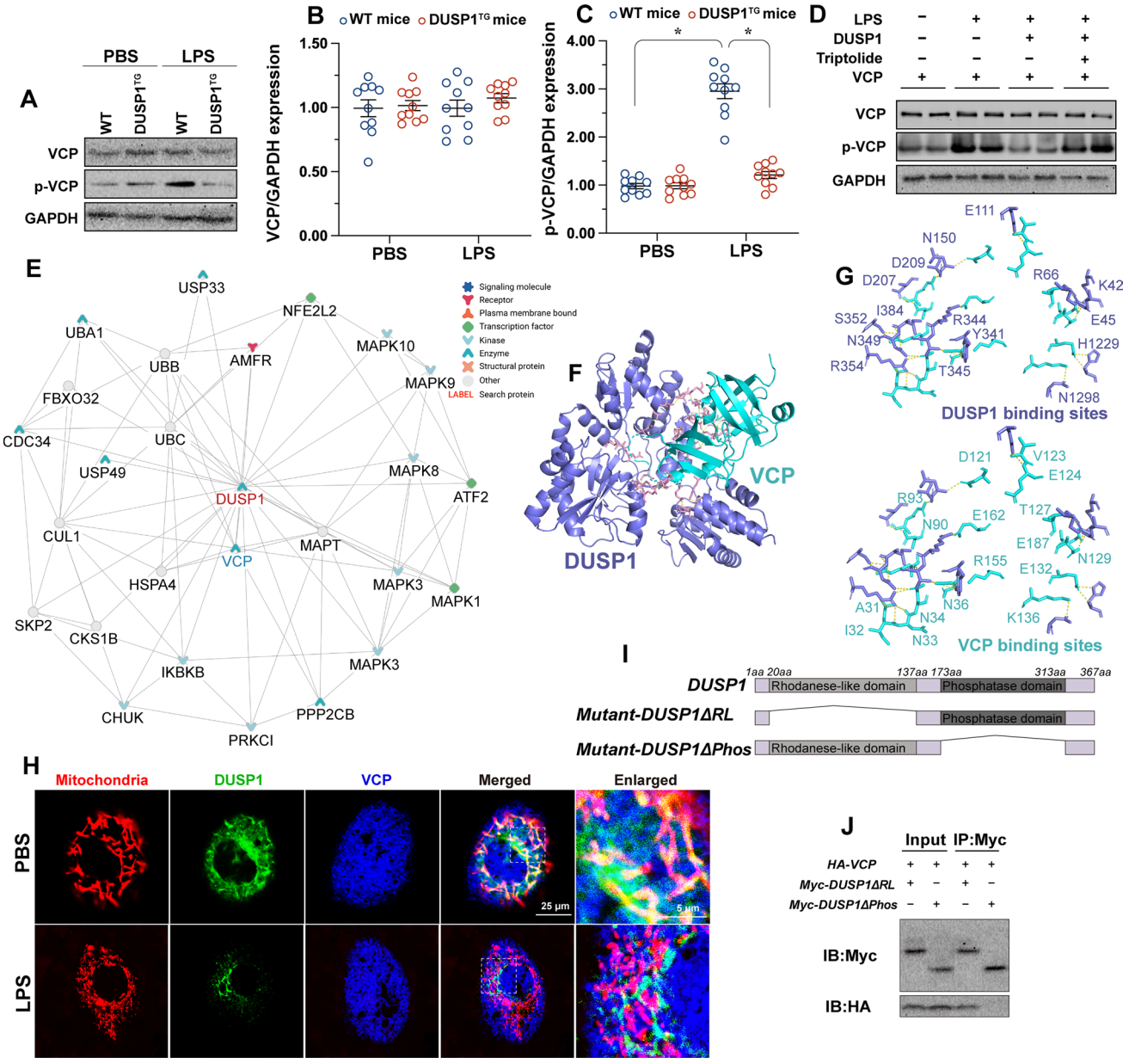

Fig. 7 DUSP1 binds to VCP and prevents LPS-mediated VCP phosphorylation. **A**–**C** Western blot analysis of total and phosphorylated (Ser784) VCP expression in cardiac lysates and cultured HL-1 cells. GAPDH was used as internal control. Data are shown as mean ± SEM (n = ten independent cell isolations per group). **D** Recombinant DUSP1 and VCP proteins were incubated together in kinase assay buffer with ATP in the presence or absence of LPS. VCP phosphorylation and DUSP1 expression were determined by western blotting. Triptolide, a DUSP1 specific inhibitor, was used to prevent DUSP1-mediated protein dephosphorylation. n = three independent cell isolations per group. **E** DUSP1/VCP interaction, as predicted by the inBio Discover tool. **F** Detailed docking model of the DUSP1/VCP interaction and corresponding docking pockets. **G** Binding sites of DUSP1 and VCP. (H) Immunofluorescent staining of VCP, DUSP1 and mitochondria in HL-1 cells in the presence or absence of LPS. n = three independent cell isolations per group. Scale bar, 25 μm. **I** Mapping of regions of DUSP1. **J** Different DUSP1 mutants were transfected into HL-1 cells. Then, immunoprecipitation, and immunoblot of cell lysates from HL-1 cells. Data are shown as mean ± SEM (n = ten independent cell isolations per group). *$p < 0.05$

cells and mitochondria in endotoxemia-caused myocardial dysfunction are mediated by preventing VCP phosphorylation. Kinase assays demonstrated that DUSP1 inhibited LPS-mediated VCP phosphorylation (Fig. 7D), and this effect could be abrogated by triptolide, a DUSP1-specific inhibitor.

To clarify the mechanism by which DUSP1 dephosphorylates VCP in the presence of LPS, we investigated whether DUSP1 directly binds to VCP and thus promotes its dephosphorylation. The protein interaction database inBio Discover (https://inbio-discover.com) indicated potential interaction

between DUSP1 and VCP (Fig. 7E). In turn, a molecular docking assay demonstrated that DUSP1 interacts with the active region of VCP (Fig. 7F). We detected the existence of H-bond interactions or hydrophobic interactions between DUSP1 and VCP (Fig. 7G). The minimum binding energy for the interaction between DUSP1 and VCP was found to be − 12.3 kcal·mol^{-1}.

Co-IP (Supporting Fig. S3A–C) assay firstly showed that the interaction between DUSP1 and VCP was impaired by LPS in cardiomyocytes. Since VCP has been showed to localize to the mitochondria or endoplasmic reticulum (ER) [34–38], we further isolated the mitochondrial fractions and ER-related proteins to determine where the interaction between DUSP1 and VCP takes place in the absence or presence of LPS. The results displayed that DUSP1 interaction with VCP primarily occurred on the mitochondria rather than on the ER (Supporting Fig. S3A-C). Immunofluorescence assay further showed that the physiological interaction between DUSP1 and VCP mainly occurred on mitochondria (Fig. 7H). The overlap between DUSP1 and VCP signals was attenuated by LPS relative to untreated cells, possibly due to a reduced expression of DUSP1 in cardiomyocyte (Fig. 7H). Further, we also observed that the localization of VCP on mitochondria were not affected by LPS although mitochondrial fragmentation was induced upon LPS (Fig. 7H).

To figure out the molecular basis of the interaction between DUSP1 and VCP, we analyzed the regions of DUSP1 that are required for cross-linking. DUSP1 possesses two major domains [39] and thus two kinds of DUSP1 domain-deletion mutants were generated (Fig. 7I). DUSP1 mutant lacking the rhodanese-like domain (DUSP1ΔRL) could interact with VCP whereas DUSP1 mutant lacking the phosphatase domain (DUSP1ΔPhos) interrupted the binding of DUSP1 and VCP (Fig. 7J). Further, transfection of DUSP1ΔRL rather than DUSP1ΔPhos was able to interrupt LPS-mediated VCP phosphorylation (Supporting Fig. S3D). Overall, our data indicate that DUSP1 phosphatase domain promotes the physiological DUSP1/VCP interaction which prevents LPS-induced VCP phosphorylation at Ser784.

Transfection of a phosphorylated VCP mutant abolishes DUSP1-mediated MQC protection

To determine whether the protective effect of DUSP1 on MQC was achieved through suppressing VCP phosphorylation, we transfected HL-1 cardiomyocytes with a phosphomimetic VCP mutant (VCP^{S784D}) in which serine 784 was replaced with aspartic acid to mimic p-VCP^{S784}. The reduction in the ratio of fragmented to normal mitochondria observed in DUSP1ΔRL-overexpressing cells treated with LPS was cancelled upon transfection with VCP^{S784D} (Fig. 8A–C). Moreover, after VCP^{S784D} transfection, DUSP1ΔRL overexpression was largely unable to restore defective mitophagy (Fig. 8D and E) and to normalize the expression of mitochondrial biogenesis markers, namely *Pgc1α* (Fig. 8F) and *Nrf1*/*Tfam1* (Fig. 8G and H) in the presence of LPS. These results indicate that induction of VCP phosphorylation abrogates the protective effects of DUSP1 on MQC in LPS-treated cardiomyocytes.

DUSP1 reduces cardiomyocyte inflammation and structural/functional abnormalities through suppressing VCP phosphorylation

We next conducted further in vitro experiments to confirm whether DUSP1-mediated cardioprotection results from preventing VCP phosphorylation. Results from qPCR assays showed that the transcriptional inhibition of pro-inflammatory factors (*Il-6*, *Mcp1*, and *Tnfα*) observed in LPS-exposed DUSP1ΔRL-overexpressing cells was nullified upon VCP^{S784D} transfection (Fig. 9A–C). Similarly, in VCP^{S784D}-transfected cardiomyocytes, DUSP1ΔRL overexpression failed to mitigate LPS-induced apoptosis (Fig. 9D and E).

Myosin immunofluorescence further showed that upon LPS exposure the stabilizing effect of DUSP1ΔRL overexpression on myosin conformation and expression was neutralized by VCP^{S784D} transfection (Fig. 9F and G). Furthermore, after VCP^{S784D} transfection, DUSP1ΔRL overexpression was unable to attenuate the LPS-induced release of TnT, CK-MB, and LDH by cultured cardiomyocytes (Fig. 9H–J). These data further confirm that DUSP1-mediated cardiomyocyte protection against LPS-induced inflammation, apoptosis, and dysfunction are abrogated by VCP phosphorylation.

Discussion

In the present study, we provided evidence for novel roles played by DUSP1 and VCP in the progression of endotoxemia-caused myocardial dysfunction. Through in vivo and in vitro experiments, in combination with genetic modification methods and gain-of-function assays, we demonstrated that DUSP1 directly binds to VCP and prevents VCP phosphorylation at Ser784, resulting in normalized MQC and improved heart function. The main relevant findings of our study can be summarized as follows: (1) LPS-induced endotoxemia downregulates cardiac DUSP1 expression; (2) overexpression of DUSP1 reduces myocardial inflammation, inhibits cardiomyocyte apoptosis, improves cardiac structural disorder, suppresses serum levels of cardiac injury markers, and increases cardiac systolic/diastolic function in vivo and contractility/relaxation parameters in vitro; (3) at the molecular level, DUSP1 overexpression sustains mitochondrial function in the presence of LPS, as evidenced by

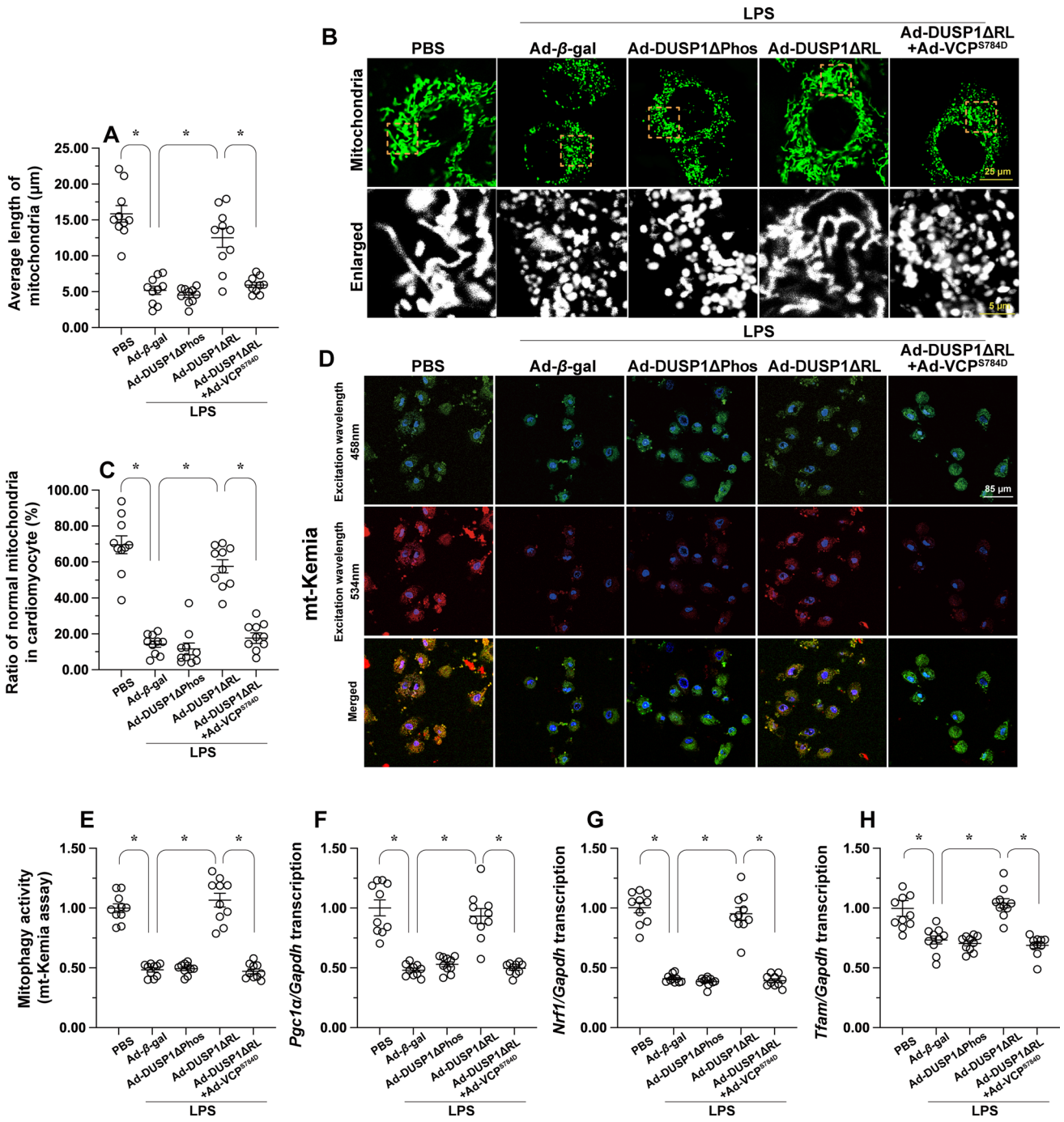

Fig. 8 Transfection of a phosphomimetic VCP mutant abolishes DUSP1-mediated MQC protection. HL-1 cells were transfected with DUSP1 mutant lacking rhodanese-like domain (22–147 amino acids) (DUSP1ΔRL), DUSP1 mutant lacking phosphatase domain (173–313 amino acids) (DUSP1ΔPhos), or a phosphomimetic VCP mutant (the serine at 784 site of VCP was replaced with aspartic acid, VCP^{S784D}) before LPS treatment. **A**–**C** Representative images of TOM20 immunofluorescence in HL-1 cardiomyocytes and quantification of average mitochondrial length and percentage of cardiomyocytes with fragmented mitochondria. Scale bar, 25 μm. **D**, **E** Detection of mitophagic activity in cardiomyocytes transfected with the mt-Keima reporter. Scale bar, 85 μm. **F**–**H** qPCR analysis of *Pgc1α*, *Nrf1* and *Tfam1* expression levels in HL-1 cardiomyocytes. *Gapdh* was used as internal control. Data are shown as mean ± SEM (n = ten independent cell isolations per group). *$p < 0.05$

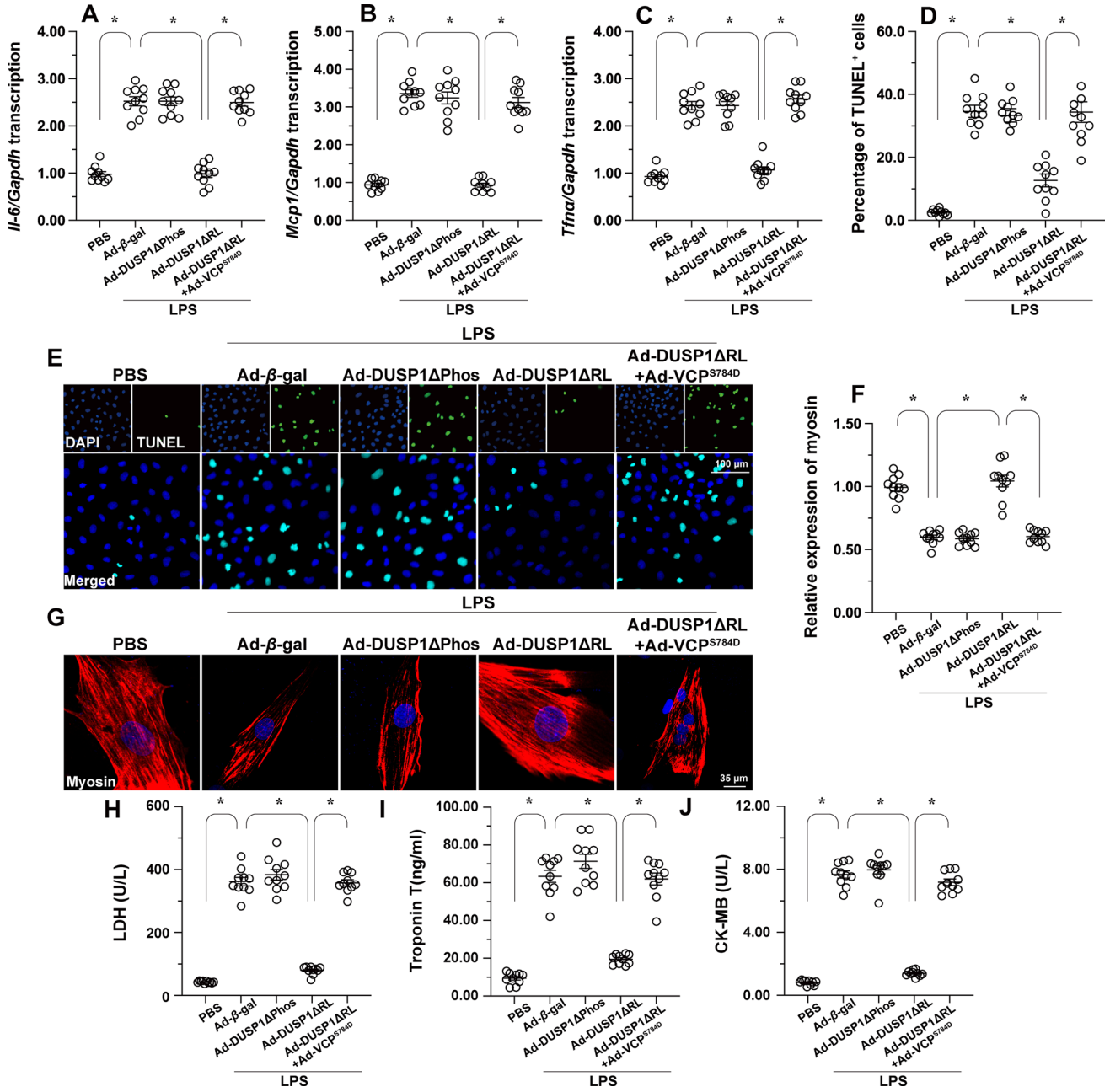

Fig. 9 DUSP1 reduces cardiomyocyte inflammation and cardiac structural and functional abnormalities by suppressing VCP phosphorylation. HL-1 cells were transfected with DUSP1 mutant lacking rhodanese-like domain (22–147 amino acids) (DUSP1ΔRL), DUSP1 mutant lacking phosphatase domain (173–313 amino acids) (DUSP1ΔPhos), or a phosphomimetic VCP mutant (the serine at 784 site of VCP was replaced with aspartic acid, VCP^{S784D}) before LPS treatment. **A**–**C** Relative *Il-6*, *Mcp1*, and *Tnfα* expression in HL-1 cells determined via qPCR. *Gapdh* was used as internal control. **D**, **E** Representative images of TUNEL staining in HL-1 cardiomyocytes and quantification of TUNEL-positive cells. Scale bar, 100 μm. **F**, **G** Representative images of myosin immunofluorescence in cultured cardiomyocytes. Myosin expression levels were normalized to those of the control group. Scale bar, 35 μm. **H**–**J**. TnT, CK-MB, and LDH levels in cell culture media were determined by ELISA. Data are shown as mean ± SEM (n = ten independent cell isolations per group). *$p < 0.05$

increased MMP, decreased mitochondrial oxidative stress, restored mitochondrial respiration, and inhibition of mPTP opening; (4) the beneficial effects of DUSP1 on mitochondrial function in LPS-treated cardiomyocytes are mediated through MQC maintenance, denoted by balanced mitochondrial fission/fusion dynamics, restored mitophagy, improved mitochondrial biogenesis, and normalized mitochondrial unfolded protein response; (5) mechanistically, DUSP1

binds to VCP and prevents LPS-mediated VCP phosphorylation at Ser784; (6) transfection of a phosphomimetic VCP mutant abolishes the protective actions of DUSP1 on MQC and on cardiomyocyte inflammation, function, and survival. Based on our findings, restoration of DUSP1 expression and suppression of VCP phosphorylation may be considered as potential targets for drug design and development for the treatment of endotoxemia-caused myocardial dysfunction.

DUSP1 was originally described as an upstream regulator of MAPK pathway molecules and consequently termed mitogen-activated protein kinase phosphatase-1 (MKP-1). Subsequent studies uncovered the anti-inflammatory effects of DUSP1 in various diseases. In *C. difficile*-induced colonic inflammation, dysregulated DUSP1 expression promotes NF-κB pathway activation, resulting in increased production of IL-1β and *Tnf*α [40]. Experiments in mouse models of septic peritonitis revealed increased lethality in global DUSP1 knockout (DUSP1$^{-/-}$) mice compared with WT animals [41]. During septic peritonitis, DUSP1$^{-/-}$ mice showed increased levels of CCL4, IL-10, and IL-6 in serum, impaired spleen and liver function, and decreased bacterial clearance [41]. An indispensable role of DUSP1 in the activation of host innate antimicrobial responses was further demonstrated in an experimental mouse model of pneumonia. Following nasal infection with the intracellular pathogen *Chlamydophila pneumoniae*, DUSP1$^{-/-}$ mice mounted an enhanced pro-inflammatory response, characterized by augmented cytokine (IL-6 and IL-1b) and chemokine (CCL3, CCL4, CXCL1, CXCL2) release and leading to increased pulmonary leukocyte infiltration [42]. In line with these findings, another study demonstrated that overexpression of DUSP1 sustained cardiomyocyte viability and reduced cardiac inflammation in a mouse model of TNF-α-induced septic cardiomyopathy [43]. However, it is necessary to point out that the pathology of endotoxemia-caused myocardial dysfunction depends not only on its associated inflammatory response; this is because anti-inflammatory approaches have failed to demonstrate clinical benefit in multiple settings, despite a strong biological rationale and supportive data from both preclinical models and some clinical pilot trials [44–46]. Importantly, clinical use of anti-TNF-α therapy with etanercept or infliximab was also not beneficial and, in some instances, appeared to be deleterious [47–49]. Accordingly, other pathological mechanisms besides inflammation must be regulated by DUSP1 to support cardiac function during endotoxemia.

MQC activation sets off an integrated stress response that involves regulation of mitochondrial fission/fusion cycles, mitophagy, and mitochondrial biogenesis. Due to the fundamental role of mitochondria in regulating cardiomyocyte contraction, growth, metabolism, signal transduction, and apoptosis, recent research has increasingly focused on the impact of MQC on various cardiovascular disorders. It has been reported that improved MQC enhances the resistance of the myocardium to I/R injury [50], myocardial infarction [51], aging-related dysfunction [52], chronic hypoxic stress [53], heart failure [54], hypertension [55], and diabetic cardiomyopathy [56]. In the present study, we provide further evidence that abnormal MQC, evidenced by disturbed mitochondrial fission/fusion, defective mitophagy, suppressed mitochondrial biogenesis, and activated mitochondrial unfolded protein response, is a key feature of endotoxemia-caused myocardial dysfunction. Our findings indicate that DUSP1 exerts cardioprotective effects through a novel role as a positive upstream regulator of MQC. This finding adds to our knowledge on the molecular function of DUSP1 and identifies the DUSP1/MQC pathway as an interventive target for the management of endotoxemia-caused myocardial dysfunction.

We found that upon LPS challenge the protective action of DUSP1 on cardiomyocytes and mitochondria was attributable to its inhibitory effect on VCP phosphorylation. VCP is an ATP-dependent protein unfoldase involved in protein degradation through cooperation with the proteasome. However, the role of VCP in cardiovascular disorders is under debate. Gain-of-function mutations in VCP have been reported to cause inclusion body myopathy associated with IBMPFD [25]. Of note, cardiac-restricted RNAi-mediated knockdown of TER94, the *Drosophila* VCP homolog, severely perturbed myofibrillar organization and heart function in adult flies [57]. These results suggested that VCP expression is necessary to maintain cardiomyocyte structure and function. Reconfirming a necessary role for VCP in cardioprotection, a study in mice demonstrated that cardiac-specific VCP overexpression significantly reduced infarct size after I/R injury [37]. Interestingly, selective inhibition of VCP through administration of KUS121 was able to reduce cardiac damage in murine and porcine models of myocardial infarction [27], suggesting that moderate inhibition of VCP function may be therapeutically relevant. In our study, we found that VCP expression in cardiomyocytes was not affected by LPS. However, LPS treatment induced VCP phosphorylation at Ser784 and this effect was prevented by DUSP1 overexpression. Importantly, forced expression of a phosphomimetic VCP mutant abolished the protective actions of DUSP1 on MQC and aggravated cardiomyocyte inflammation, apoptosis, and mechanical function. In line with these findings, recent evidence revealed that VCP phosphorylation at Ser784 is a clinically relevant enhancer of VCP function in the progression of various diseases and hence a potential therapeutic target. For instance, increased VCP phosphorylation was associated with sorafenib-mediated hepatocellular carcinoma cell death [58]. Consistently, slower tumor growth, associated with apoptosis induction, was observed in nude mice implanted with phosphomimetic

VCP^{T76A}-reconstituted cancer cells, compared to control mice bearing VCP^{WT}-expressing tumors [59].

There are several limitations in the present study. First, we used a high dose of LPS (20 mg/kg) to induce endotoxemia-caused myocardial dysfunction based on our previous works [10, 60, 61]. In addition, there are several studies also used a high concentration of LPS (20 mg/kg) to establish a sepsis-related multiple organs dysfunction model in vivo, such as septic kidney injury[62] and septic cardiomyopathy [63, 64]. In fact, a low dose of LPS often causes endotoxemia, not sepsis, an effect that is followed by systolic inflammation response. By comparison, a high dose of LPS always induces the sepsis-related complications in 1 or 2 days. Second, recent studies [65] have reported that lower doses of LPS stimulate autophagy/mitophagy during endotoxin-induced cardiomyopathy, and that this adaptive response is diminished at higher doses. Sun et al. found [65] that low concentrations of LPS (0.25 mg/kg, 0.5 mg/kg, 1.0 mg/kg, 1.5 mg/kg, and 2.5 mg/kg) seem to dose-dependently elevate LC3II expression and promote p62 degradation in LPS-induced septic cardiomyopathy. However, high concentrations of LPS (5.0 mg/kg, 10 mg/kg, and 15 mg/kg) are able to dose-dependently repress LC3II formation and thus accelerate p62 accumulation. These results suggest that lower LPS doses-caused mild inflammation response may be an inducer of autophagy/mitophagy, and that higher LPS concentrations-mediated multiple organs inflammatory cascades are correlated with a depression of autophagy/mitophagy. Although our results are similar to the previous findings [65], it requires more data to show the cardioprotective effects of DUSP1 during endotoxemia induced by a low dose of LPS.

In conclusion, our results demonstrated that DUSP1 functions as a protective factor against endotoxemia-mediated myocardial injury through normalizing mitochondrial function. At the molecular level, DUSP1 directly binds to VCP and prevents LPS-mediated VCP phosphorylation at Ser784, resulting into improved MQC and normalized cardiac function. Our findings highlight DUSP1/VCP/MQC as a novel pathway involved in the pathogenesis of endotoxemia-caused myocardial dysfunction and may thus help advance new strategies to prevent myocardial damage and mitochondrial dysfunction associated with this condition.

Materials

Animals

All procedures related to animal treatment and surgery were approved by the Chinese PLA General Hospital. Male mice (aged 8–10 weeks) from a C57BL/6J genetic background were bred and housed in individually vented cages under ABSL-2 conditions in the Chinese PLA General Hospital Animal Center. DUSP1 transgenic ($DUSP1^{TG}$) mice were established as previously described [14]. Briefly, the pBSII-12.4kbVill-DUSP1 plasmids were obtained from OriGene (Rockville, MD, USA). Then, the pBSII-12.4kbVillDUSP1 plasmids were digested with EcoRI and KpnI to obtain villinDUSP1 DNA fragments. Then the transgene was purified and injected into mouse blastocysts to generate transgenic mice. Mice were sacrificed at their respective endpoint studies by removal of vital organs under deep anesthesia with ketamine (100 mg/kg, i.p.) and xylazine (10 mg/kg, i.p.). No animals were excluded due to premature death or failure to achieve the predicted phenotypes. Mice were injected intraperitoneally with a single dose of lipopolysaccharide (20 mg/kg, Sigma-Aldrich, St. Louis, MO, USA) dissolved in phosphate buffer saline for 48 h to induce endotoxemia-caused myocardial dysfunction based on our previous studies [10, 61] and recent experiments [63, 64]. Mice administered an equal volume of phosphate buffer saline served as controls. Blood samples were collected with EDTA (1.8 mg/ml) and centrifuged (400 rpm, 20 min, 4 °C) to separate plasma. Heart tissues were removed rapidly and stored at − 80 °C for further analysis.

ELISA and seahorse assay

Serum Creatine Kinase MB (CK-MB) (BioVision, MA, USA), Troponin T (TNT) (MyBioSource, Inc., San Diego, CA, USA), and Lactate Dehydrogenase (LDH) (MyBioSource, Inc., San Diego, CA, USA) were measured by Colorimetric/Fluorometric Assay Kits. ELISA was used to determine caspase-3 activity (MyBioSource, Inc., San Diego, CA, USA) and ATP production (MyBioSource, Inc., San Diego, CA, USA) according to the manufacturers' instructions. The Agilent Seahorse XF real-time ATP rate assay was performed using an XF-24 Extracellular Flux Analyzer (Agilent Technologies) once HL-1 cells reached 95% confluence (4×10^4/well) on XF24 Cell Culture Microplates (Agilent, Santa Clara, CA, USA). Medium was replaced with unbuffered XF medium (Agilent, Santa Clara, CA, USA), and cells were equilibrated for 1 h at 37 °C without CO_2. XF24 Sensor Cartridges were pre-hydrated overnight in calibration buffer, then loaded with XF Real-Time ATP Rate Assay compounds (final concentrations: 2.5 µg/mL oligomycin, 2 µM rotenone, 4 µM antimycin A). Integrated sensor cartridges and cell culture microplates were inserted into XF96 Analyzer and subjected to built-in XF Real-Time ATP Rate Assay protocol. Data were analyzed by Agilent ATP Assay Report Generator, with statistical analysis by GraphPad Prism 7 software (La Jolla, CA, USA).

Transmission electron microscopy

Transmission electron microscopy (TEM) was applied for ultrastructural analysis of cardiac tissues [66]. Samples were fixed in a 1.6% glutaraldehyde solution in 0.1 M sodium phosphate buffer at room temperature (RT) and stored overnight at 4 °C. After triple rinsing in 0.1 M cacodylate buffer (15 min/rinse), cells were postfixed in 1% osmium tetroxide and 1% potassium ferrocyanide solution in 0.1 M cacodylate buffer for 1 h at RT. Samples were subsequently dehydrated in a series of acetone baths (90% and 100%, three times, 15 min each) and progressively embedded in Epon 812 resin (acetone/resin 1:1, 100% resin, two times, 2 h/bath). Resin blocs were finally left to harden in a 60 °C oven for 2 days. Ultrathin sections (70 nm) were obtained with a Reichert Ultracut S ultramicrotome equipped with a Drukker International diamond knife and collected on 200 mesh copper grids. Sections were stained with lead citrate and uranyl acetate. TEM was performed with a JEOL JEM-1400 microscope equipped with a Morada camera (CLSM, Olympus, Japan), at a 100 kV accelerating voltage.

Cell culture

Immortalized mouse cardiac muscle HL-1 cells were obtained from American Type Culture Collection (Manassas, VA, USA). Cells were cultured in Dulbecco's Modified Eagle Medium (DMEM) with glutamine at 37 °C in a 5% CO_2 incubator. The media were supplemented with 10% FBS and 100 µg/ml penicillin/streptomycin. The HL-1 cell line was authenticated by short tandem repeats (STRs) DNA profiling. To induce endotoxemia in vitro, HL-1 cells were treated with 10 µg/mL of LPS for 24 h according to our previous studies [10, 61].

Cardiomyocyte isolation and contractility analysis

Mouse hearts were dissected and retrogradely perfused with HEPES-Tyrode's buffer (130 mM NaCl, 5.4 mM KCl, 0.5 mM $MgCl_2$, 0.33 mM NaH_2PO_4, 0.25 mM HEPES, 22 mM glucose; 37 °C; pH 7.4) containing 100 mg/ml collagenase type 2 using the Langendorff method. Hearts were then mechanically sheared and filtered through a 100-mm mesh filter. The single-cell suspension was centrifuged at 200 rpm for 3 min. The pellets, which contained the majority of cardiomyocytes, were washed twice with HEPES-Tyrode's buffer containing $CaCl_2$ and were collected after centrifugation at 200 rpm. Contractility measurements were performed in field-stimulated cells at a pace of 1 Hz using an IonOptix Fluorescence and Contractility System (IonOptix, MA, USA) as previously described [66, 67]. Contractions were elicited by rectangular depolarizing pulses, 2 ms in duration and twice-diastolic threshold in intensity, by platinum electrodes. Cell shortening was measured by edge-track detection, and calcium transients were measured by epifluorescence after loading the cardiomyocytes with 1 µM Fura-2 AM (Thermo Fisher Scientific, MA, USA) for 10 min. Contractility and calcium transients were recorded, and 5 to 10 consecutive single-cell contractions during steady state were analyzed using IonWizard software (IonOptix, MA, USA).

Echocardiography

Cardiac function was determined via echocardiography (FUJIFILM VisualSonics Inc., Toronto, Canada,). After alignment in the transverse B-mode with the papillary muscles, cardiac function was measured on M-mode images. Echocardiography results were analyzed blindly.

Immunofluorescence staining

Cells were grown in 4-well chamber glass slides for 48 h (24 h in media with 10% FBS and an additional 24 h in media without serum). Primary antibodies against TOM20 (1:500, #ab78547, Abcam, Cambridge, MA, USA) and Myosin IIB (1:500; #ab254472, Abcam, Cambridge, MA, USA) were used in cultured cells. Heart tissues were fixed with 4% paraformaldehyde, embedded in paraffin, sectioned, and permeabilized with 0.1% saponin prior to incubation with GR1 (1:500, #ab25377, Abcam, Cambridge, MA, USA) and TnT (1:500; #MBS533262, MyBioSource, Inc., San Diego, CA, USA) antibodies. Indirect fluorescent detection was done through incubation with goat IgG (H + L) highly cross-adsorbed secondary antibody-Alexa Fluor™ Plus 647 (1:2000, #A32733, Thermo Fisher Scientific, MA, USA), goat IgG (H + L) highly cross-adsorbed secondary antibody-Alexa Fluor™ Plus 488 (1:2000, #A48262, Thermo Fisher Scientific, MA, USA), goat IgY (H + L) cross-adsorbed secondary antibody-Alexa Fluor™ Plus 405 (1:2000, #A48260, Thermo Fisher Scientific, MA, USA). Nuclei were stained with DAPI. The stained slides were examined under a Zeiss Axio Observer microscope with Apotome attachment (Oberkochen, Germany).

ICAM1 immunohistochemistry

Heart tissues were fixed in 4% PFA overnight, dehydrated in ethanol, and embedded in paraffin. Immunohistochemistry was performed using an ICAM1 (1:500;#179707, Abcam, Cambridge, MA, USA) antibody. HRP-conjugated anti-mouse secondary antibodies were then applied. Images were acquired using a Vectra 2 Multispectral Imaging System (PerkinElmer, Shanghai, China) and ICAM1-positive cells were quantified using NIH Image J2 software.

Mitochondrial fractions and endoplasmic reticulum (ER) fractions extraction assays

For mitochondrial protein lysates, mitochondrial fractions from HL-1 cells were isolated using the Mitochondria Isolation Kit (Thermo Fisher Scientific, MA, USA) according to manufacturer's protocol. In brief, cells were harvested, rinsed with PBS, and suspended in isolation buffer (3 mM Hepes–KOH (pH 7.4), 0.21 M mannitol, 0.07 M sucrose, 0.2 mM EGTA) on ice. Then, homogenates were overlaid on 0.34 M sucrose followed by centrifugation at 500 rpm. These steps were repeated for three times before centrifugation of supernatants at 10,000 rpm to extract mitochondrial fractions. Endoplasmic reticulum (ER) fractions from HL-1 cells were isolated using the Endoplasmic Reticulum Isolation Kit (Sigma-Aldrich, St. Louis, MO, USA). Briefly, cells were harvested, rinsed with PBS, and centrifuged for 5 min at 4 °C at 500 rpm. The supernatant was removed and the pellet resuspended in 1 ml buffer E (20 mM Hepes, pH 7.4, 250 mM sucrose, 1 mM EDTA, and protease inhibitor cocktail) for 15 min. After centrifugation of supernatants at 4 °C for three times (centrifugation at 10,000 rpm for 5 min, centrifugation at 80,000 rpm for 20 min, and centrifugation at 100,000 rpm for 1 h), the supernatant was removed and retained as the soluble fraction, and the pellet was retained as the ER fraction for analysis.

Immunoprecipitation and immunoblotting assays

Heart tissues or HL-1 cardiomyocytes were homogenized in ice-cold lysis buffer (25 mM Tris pH 8.0, 150 mM NaCl, 1 mM $CaCl_2$, 1% Triton X-100) with EDTA-free protease inhibitors. Proteins were precipitated by centrifugation at 4 °C, 12,000 rpm for 10 min and concentrations determined using a BCA assay kit. For immunoblotting experiments, proteins were separated on 10% SDS–polyacrylamide gels, transferred to PVDF membranes (Millipore, Germany), and probed with primary antibodies overnight. For immunoprecipitation (IP) experiments, primary antibodies and cell lysates were co-incubated overnight at 4 °C, and immunoprecipitated complexes were captured by incubation for 6 h at 4 °C with Protein A/G PLUS-Agarose beads (Santa Cruz Biotechnology, Inc., Texas, USA; pre-blocked with 0.1% BSA for 1 h at 4 °C). Beads were washed with wash buffer (50 mM Tris–HCl, 400 mM NaCl, and 0.8% Triton-X-100, pH 7.5) 3–5 times by centrifugation (300 rpm, 4 min at 4 °C). For co-IP experiments, IP samples were quantified and incubated overnight at 4 °C with magnetic beads coated with primary antibodies. After 5 washes, bound proteins were eluted in sample buffer at 95 °C for 10 min, separated by SDS-PAGE, and transferred to PVDF membranes for immunoblotting. Primary antibodies included: DUSP1 (1:1000; #ab217347, Abcam, Cambridge, MA, USA), PGC-1α (1:1000; #ab188102, Abcam, Cambridge, MA, USA), DRP1 (1:1000; #ab184247, Abcam, Cambridge, MA, USA), FIS1 (1:1000; #ab156865, Abcam, Cambridge, MA, USA), MFN2 (1:1000; #ab124773, Abcam, Cambridge, MA, USA), OPA1 (1:1000; #ab42364, Abcam, Cambridge, MA, USA), GAPDH (1:1000; #ab8245, Abcam, Cambridge, MA, USA), TOM20 (1:1000; #ab186735, Abcam, Cambridge, MA, USA), ATG5 (1:1000; #ab108327, Abcam, Cambridge, MA, USA), VCP (1:1000; #ab109240, Abcam, Cambridge, MA, USA), p-VCP^{Ser784} (1:1000; #OAAF00581-Biotin, Aviva Systems Biology, San Diego, CA, USA), PARKIN (1:1000; #ab77924, Abcam, Cambridge, MA, USA), BECLIN1 (1:1000; #ab207612, Abcam), LC3 (1:1000, #ab192890, Abcam, Cambridge, MA, USA), p62 (1:1000, #ab109012, Abcam, Cambridge, MA, USA), and TIM23 (1:1000, #ab230253, Abcam, Cambridge, MA, USA).

Real-time quantitative PCR

Total RNA from 10 mg heart tissue was extracted with TRIzol reagent (Invitrogen) followed by chloroform purification and isopropanol precipitation. RNA concentration was measured using a NanoDrop instrument (Thermo Fisher Scientific, MA, USA). RNA was reverse transcribed using PrimeScript™ RT Reagent Kit (Takara Bio Inc., Beijing, China) and the resulting cDNA was amplified using a Fast Real-Time PCR instrument (ABI-7900–384, Applied Biosystems, Thermo Fisher Scientific, MA, USA) with TB Green Premix Ex Taq™ II (RR820A, Takara, Japan). The *Cytochrome c oxidase subunit I (Co1)* gene of the mtDNA and the *NADH: Ubiquinone oxidoreductase core subunit v1* (*Ndufv1)* nDNA gene were amplified by qPCR. The reaction was initiated at 94 °C for 10 min, followed by 40 cycles through 94 °C × 10 s, 60 °C × 30 s, and 94 °C × 10 s. All reactions were run in duplicate. Amplification curves were analyzed using SDS 1.9.1 software (Applied Biosystems, Thermo Fisher Scientific, MA, USA), and these curves were used to determine the relative mtDNA: nDNA ratio in each sample based on a previous study [68]. The following primer pairs were used: *Tnfα* (Forward, 5′-AGATGGAGCAACCTAAGGTC-3′; Reverse, 5′-GCAGACCTCGCTGTTCTAGC-3′), *Il-6* (Forward, 5′-CAGACTCGCGCCTCTAAGGAGT-3′; Reverse, 5′-GATAGCCGATCCGTCGAA-3′), *Mcp1* (Forward, 5′-GGATGGATTGCACAGCCATT-3′; Reverse, 5′-GCGCCGACTCAGAGGTGT-3′), *Nrf1* (Forward, 5′-GCACCTTTGGAGAATGTGGT-3′; Reverse, 5′-CTGAGCCTGGGTCATTTTGT-3′), *Tfam* (Forward, 5′-GGCGAATTCCTCGAGGCCACCATGGCGCTGTTCCGGGGAATGT-3′; Reverse, 5′-CATACGCGTATGCTCAGAGATGTCTCCGGATCGT-3′), *Lonp1* (Forward, 5′-GGTTGAGAATGTAGCCCATGA-3′; Reverse, 5′-CGATGATATCCCGAATGGTC-3′), *Mthsp70* (Forward, 5′-CTCTGGGAGGCGTCTTTACC-3′; Reverse, 5′-CGTTCCCCC

TGACACACTTT-3′), *Atf6* (Forward, 5′-TTATCAGCA TACAGCCTGCG-3′; Reverse, 5′-CTTGGGACTTTG AGCCTCTG-3′), *Co1* (Forward, 5′-TGCTAGCCGCAG GCA TTAC-3′; Reverse, 5′-GGGTGCCCAAAGAATCAG AAC-3′), *Ndufv1* (Forward, 5′- CTTCCCCACTGGCCT CAAG-3′; Reverse, 5′-CCAAAACCCAGTGATCCAGC-3′).

Adenoviral vector construction and plasmid infection

DUSP1 and VCP expression plasmids were constructed by cloning the open reading frame of each cDNA into the multiple cloning sites of pcDNA3.0 vectors with HA-tag or Myc-tag epitope sequences. DUSP1 lacking rhodanese-like domain (22–147 amino acids) (DUSP1ΔRL), DUSP1 lacking phosphatase domain (173–313 amino acids) (DUSP1ΔPhos), and full length (1–367 amino acids) of DUSP1 were amplified using PCR and the produces were introduced into pcDNA3.1/Myc (Invitrogen) to construct the Myc-DUSP1 mutants. Plasmids encoding a phosphomimetic VCP mutant (pcDNA3.0-ALDOB-R46A and K108A) were constructed by replacing serine 784 with aspartic acid (VCP^{S784D}) as previously described [61, 69]. A recombinant adenovirus vector encoding the mouse *Dusp1* gene was constructed and transfected into HEK293 cells to generate Ad-DUSP1 adenovirus for DUSP1 overexpression in HL-1 cells. Adenoviruses were generated using an AdEasy Adenoviral Vector System Kit (Agilent Technologies, Thermo Fisher Scientific, MA, USA). Recombinant adenoviruses were plaque purified and tittered to 10^{10} plaque-forming units (PFU) per ml. The verification of virus production was based on a restriction enzyme-mediated DNA analysis of plaque purified virus. Adenovirus encoding β-gal (Ad-β-gal) was used as a control.

TUNEL staining, mitochondrial ROS detection, and mitochondrial membrane potential (MMP) measurement

TUNEL staining was performed using a Click-iT™ Plus TUNEL Assay Kit for In Situ Apoptosis Detection (Thermo Fisher Scientific, MA, USA). Mitochondrial ROS was detected using the MitoSOX Red mitochondrial superoxide indicator (Thermo Fisher Scientific, MA, USA). MMP was analyzed using a JC-1 Mitochondrial Potential Sensor (Thermo Fisher Scientific, MA, USA).

Kinase activity and molecular docking assays

For in vitro kinase assay, Recombinant DUSP1 Protein (Novus Biologicals, LLC., Toronto, Canada) and Recombinant VCP Protein (Novus Biologicals, LLC., Toronto, Canada) were incubated together in kinase assay buffer (Cell Signaling Technology) with adenosine 5′-triphosphate (ATP), according to the manufacturer's instructions. Triptolide (Selleck Chemicals, Shanghai, Beijing) was used to prevent the activity of DUSP1. The Schrödinger 2017-1 suite (Schrödinger Inc., New York, NY, USA) was employed to perform the docking analysis. The DUSP1 and VCP structures were retrieved from the available crystal structures and prepared for docking following the protein Preparation Wizard workflow in the Maestro package. The binding site was selected using the Grid Generation procedure. The prepared ligand was flexibly docked into the receptor using Glide (XP mode) with default parameters. Microscale thermophoresis (MST) was applied to determine binding affinity between VCP and DUSP1.

Statistical analysis

Results were analyzed using GraphPad Prism 5.0 statistical software. Data are shown as means ± standard error of the mean (SEM). For comparisons between two groups, parametric Student t-test or nonparametric Mann–Whitney test were used. For comparisons between more than two groups, parametric one-way ANOVA test followed by Bonferroni test was used. Histopathological parameters were statistically analyzed using Chi-square test. $P < 0.05$ was considered significant.

Supplementary Information The online version contains supplementary material available at https://doi.org/10.1007/s00018-023-04863-z.

Author contributions JW and HZ conceived the original experiments. TX and YL contributed to the manuscript revision. SC and RH, and HZ, carried out all the in vivo experiments and molecular investigation in vitro. HZ and MZ wrote the whole manuscript. HZ, MZ, HZ revised the final version of manuscript. All the authors read the article and approved the submission.

Funding This study was supported by grants from the NSFC (Nos. 82270279 and 82200296) and Youth Innovative Talents Training Program of Tianjin First Central Hospital Young Talents.

Data availability The data supporting the findings of this study are found within the article and the supplementary material. All relevant raw data will be made available from the corresponding author upon reasonable request.

Declarations

Conflict of interest The authors declared no conflict of interest.

Ethical statement Experiments were performed under a project license (Beijing, China) granted by the committee on the Ethics of Chinese PLA General Hospital, in compliance with the Guidelines for the Management and Use of Laboratory Animals.

References

1. Vieillard-Baron A (2011) Septic cardiomyopathy. Ann Intensive Care 1:6
2. Martin L, Derwall M, Al Zoubi S, Zechendorf E, Reuter DA, Thiemermann C, Schuerholz T (2019) The septic heart: current understanding of molecular mechanisms and clinical implications. Chest 155:427–437
3. Tan Y, Chen S, Zhong J, Ren J, Dong M (2019) Mitochondrial injury and targeted intervention in septic cardiomyopathy. Curr Pharm Des 25:2060–2070
4. Cimolai MC, Alvarez S, Bode C, Bugger H (2015) Mitochondrial mechanisms in septic cardiomyopathy. Int J Mol Sci 16:17763–17778
5. Shang X, Zhang Y, Xu J, Li M, Wang X, Yu R (2020) SRV2 promotes mitochondrial fission and Mst1-Drp1 signaling in LPS-induced septic cardiomyopathy. Aging (Albany NY) 12:1417–1432
6. Durand A, Duburcq T, Dekeyser T, Neviere R, Howsam M, Favory R, Preau S (2017) Involvement of mitochondrial disorders in septic cardiomyopathy. Oxid Med Cell Longev 2017:4076348
7. Ji L, He Q, Liu Y, Deng Y, Xie M, Luo K, Cai X, Zuo Y, Wu W, Li Q, Zhou R, Li T (2022) Ketone body β-hydroxybutyrate prevents myocardial oxidative stress in septic cardiomyopathy. Oxid Med Cell Longev 2022:2513837
8. Zhong J, Tan Y, Lu J, Liu J, Xiao X, Zhu P, Chen S, Zheng S, Chen Y, Hu Y, Guo Z (2019) Therapeutic contribution of melatonin to the treatment of septic cardiomyopathy: a novel mechanism linking Ripk3-modified mitochondrial performance and endoplasmic reticulum function. Redox Biol 26:101287
9. Jiang X, Cai S, Jin Y, Wu F, He J, Wu X, Tan Y, Wang Y (2021) Irisin attenuates oxidative stress, mitochondrial dysfunction, and apoptosis in the H9C2 cellular model of septic cardiomyopathy through augmenting Fundc1-dependent mitophagy. Oxid Med Cell Longev 2021:2989974
10. Wang Y, Jasper H, Toan S, Muid D, Chang X, Zhou H (2021) Mitophagy coordinates the mitochondrial unfolded protein response to attenuate inflammation-mediated myocardial injury. Redox Biol 45:102049
11. Teng CH, Huang WN, Meng TC (2007) Several dual specificity phosphatases coordinate to control the magnitude and duration of JNK activation in signaling response to oxidative stress. J Biol Chem 282:28395–28407
12. Shen J, Zhang Y, Yu H, Shen B, Liang Y, Jin R, Liu X, Shi L, Cai X (2016) Role of DUSP1/MKP1 in tumorigenesis, tumor progression and therapy. Cancer Med 5:2061–2068
13. Keyse SM (2008) Dual-specificity MAP kinase phosphatases (MKPs) and cancer. Cancer Metastasis Rev 27:253–261
14. Jin Q, Li R, Hu N, Xin T, Zhu P, Hu S, Ma S, Zhu H, Ren J, Zhou H (2018) DUSP1 alleviates cardiac ischemia/reperfusion injury by suppressing the Mff-required mitochondrial fission and Bnip3-related mitophagy via the JNK pathways. Redox Biol 14:576–587
15. Bermúdez-Muñoz JM, Celaya AM, García-Mato Á, Muñoz-Espín D, Rodríguez-De La Rosa L, Serrano M, Varela-Nieto I (2021) Dual-specificity phosphatase 1 (DUSP1) has a central role in redox homeostasis and inflammation in the mouse cochlea. Antioxidants (Basel) 10:1351
16. Sheng J, Li H, Dai Q, Lu C, Xu M, Zhang J, Feng J (2019) DUSP1 recuses diabetic nephropathy via repressing JNK-Mff-mitochondrial fission pathways. J Cell Physiol 234:3043–3057
17. Hou X, Li L, Chen S, Ge C, Shen M, Fu Z (2021) MKP-1 overexpression reduces postischemic myocardial damage through attenuation of ER stress and mitochondrial damage. Oxid Med Cell Longev 2021:8905578
18. Huang D, Jiang Y (2020) MKP1 reduces neuroinflammation via inhibiting endoplasmic reticulum stress and mitochondrial dysfunction. J Cell Physiol 235:4316–4325
19. Lawan A, Min K, Zhang L, Canfran-Duque A, Jurczak MJ, Camporez JPG, Nie Y, Gavin TP, Shulman GI, Fernandez-Hernando C, Bennett AM (2018) Skeletal muscle-specific deletion of MKP-1 reveals a p38 MAPK/JNK/Akt signaling node that regulates obesity-induced insulin resistance. Diabetes 67:624–635
20. Ding YH, Miao RX, Zhang Q (2021) Hypaphorine exerts anti-inflammatory effects in sepsis induced acute lung injury via modulating DUSP1/p38/JNK pathway. Kaohsiung J Med Sci 37:883–893
21. Hammer M, Mages J, Dietrich H, Servatius A, Howells N, Cato AC, Lang R (2006) Dual specificity phosphatase 1 (DUSP1) regulates a subset of LPS-induced genes and protects mice from lethal endotoxin shock. J Exp Med 203:15–20
22. Zhang J, Xu X, Wang M (2021) Clinical significance of serum miR-101-3p expression in patients with neonatal sepsis. Per Med 18:541–550
23. Brudecki L, Ferguson DA, Mccall CE, El Gazzar M (2013) Mitogen-activated protein kinase phosphatase 1 disrupts proinflammatory protein synthesis in endotoxin-adapted monocytes. Clin Vaccine Immunol 20:1396–1404
24. Frazier WJ, Wang X, Wancket LM, Li XA, Meng X, Nelin LD, Cato AC, Liu Y (2009) Increased inflammation, impaired bacterial clearance, and metabolic disruption after gram-negative sepsis in Mkp-1-deficient mice. J Immunol 183:7411–7419
25. Watts GD, Wymer J, Kovach MJ, Mehta SG, Mumm S, Darvish D, Pestronk A, Whyte MP, Kimonis VE (2004) Inclusion body myopathy associated with Paget disease of bone and frontotemporal dementia is caused by mutant valosin-containing protein. Nat Genet 36:377–381
26. Nalbandian A, Llewellyn KJ, Gomez A, Walker N, Su H, Dunnigan A, Chwa M, Vesa J, Kenney MC, Kimonis VE (2015) In vitro studies in VCP-associated multisystem proteinopathy suggest altered mitochondrial bioenergetics. Mitochondrion 22:1–8
27. Ide Y, Horie T, Saito N, Watanabe S, Otani C, Miyasaka Y, Kuwabara Y, Nishino T, Nakao T, Nishiga M, Nishi H, Nakashima Y, Nakazeki F, Koyama S, Kimura M, Tsuji S, Rodriguez RR, Xu S, Yamasaki T, Watanabe T, Yamamoto M, Yanagita M, Kimura T, Kakizuka A, Ono K (2019) Cardioprotective effects of VCP modulator KUS121 in murine and porcine models of myocardial infarction. JACC Basic Transl Sci 4:701–714
28. Guo X, Sun X, Hu D, Wang YJ, Fujioka H, Vyas R, Chakrapani S, Joshi AU, Luo Y, Mochly-Rosen D, Qi X (2016) VCP recruitment to mitochondria causes mitophagy impairment and neurodegeneration in models of Huntington's disease. Nat Commun 7:12646
29. Ogor P, Yoshida T, Koike M, Kakizuka A (2021) VCP relocalization limits mitochondrial activity, GSH depletion and ferroptosis during starvation in PC3 prostate cancer cells. Genes Cells 26:570–582
30. Kim NC, Tresse E, Kolaitis RM, Molliex A, Thomas RE, Alami NH, Wang B, Joshi A, Smith RB, Ritson GP, Winborn BJ, Moore J, Lee JY, Yao TP, Pallanck L, Kundu M, Taylor JP (2013) VCP is essential for mitochondrial quality control by PINK1/Parkin and this function is impaired by VCP mutations. Neuron 78:65–80
31. Yu CC, Yang JC, Chang YC, Chuang JG, Lin CW, Wu MS, Chow LP (2013) VCP phosphorylation-dependent interaction partners

prevent apoptosis in *Helicobacter pylori*-infected gastric epithelial cells. PLoS ONE 8:e55724
32. Shao J (2020) Ser(784) phosphorylation: a clinically relevant enhancer of VCP function in the DNA damage response. Mol Cell Oncol 7:1796179
33. Zhu C, Rogers A, Asleh K, Won J, Gao D, Leung S, Li S, Vij KR, Zhu J, Held JM, You Z, Nielsen TO, Shao J (2020) Phospho-Ser(784)-VCP is required for dna damage response and is associated with poor prognosis of chemotherapy-treated breast cancer. Cell Rep 31:107745
34. Sun X, Zhou N, Ma B, Wu W, Stoll S, Lai L, Qin G, Qiu H (2021) Functional inhibition of valosin-containing protein induces cardiac dilation and dysfunction in a new dominant-negative transgenic mouse model. Cells 10:2891
35. Brody MJ, Vanhoutte D, Bakshi CV, Liu R, Correll RN, Sargent MA, Molkentin JD (2019) Disruption of valosin-containing protein activity causes cardiomyopathy and reveals pleiotropic functions in cardiac homeostasis. J Biol Chem 294:8918–8929
36. Zhou N, Chen X, Xi J, Ma B, Leimena C, Stoll S, Qin G, Wang C, Qiu H (2020) Novel genomic targets of valosin-containing protein in protecting pathological cardiac hypertrophy. Sci Rep 10:18098
37. Lizano P, Rashed E, Stoll S, Zhou N, Wen H, Hays TT, Qin G, Xie LH, Depre C, Qiu H (2017) The valosin-containing protein is a novel mediator of mitochondrial respiration and cell survival in the heart in vivo. Sci Rep 7:46324
38. Zhou N, Stoll S, Qiu H (2017) VCP represses pathological cardiac hypertrophy. Aging (Albany NY) 9:2469–2470
39. Kho DH, Uddin MH, Chatterjee M, Vogt A, Raz A, Wu GS (2019) GP78 cooperates with dual-specificity phosphatase 1 to stimulate epidermal growth factor receptor-mediated extracellular signal-regulated kinase signaling. Mol Cell Biol 39:e00485-18
40. Li Y, Xu S, Xu Q, Chen Y (2020) Clostridium difficile toxin B induces colonic inflammation through the TRIM46/DUSP1/MAPKs and NF-κB signalling pathway. Artif Cells Nanomed Biotechnol 48:452–462
41. Hammer M, Echtenachter B, Weighardt H, Jozefowski K, Rose-John S, Männel DN, Holzmann B, Lang R (2010) Increased inflammation and lethality of Dusp1-/- mice in polymicrobial peritonitis models. Immunology 131:395–404
42. Rodriguez N, Dietrich H, Mossbrugger I, Weintz G, Scheller J, Hammer M, Quintanilla-Martinez L, Rose-John S, Miethke T, Lang R (2010) Increased inflammation and impaired resistance to Chlamydophila pneumoniae infection in Dusp1(-/-) mice: critical role of IL-6. J Leukoc Biol 88:579–587
43. Chang W, Feng M, Li Y, Sun Y, Sun L (2019) MKP1 overexpression reduces TNF-α-induced cardiac injury via suppressing mitochondrial fragmentation and inhibiting the JNK-MIEF1 pathways. J Cell Physiol. https://doi.org/10.1002/jcp.28273
44. Cooper LT, Hare JM, Tazelaar HD, Edwards WD, Starling RC, Deng MC, Menon S, Mullen GM, Jaski B, Bailey KR, Cunningham MW, Dec GW (2008) Usefulness of immunosuppression for giant cell myocarditis. Am J Cardiol 102:1535–1539
45. Frustaci A, Russo MA, Chimenti C (2009) Randomized study on the efficacy of immunosuppressive therapy in patients with virus-negative inflammatory cardiomyopathy: the TIMIC study. Eur Heart J 30:1995–2002
46. Wojnicz R, Nowalany-Kozielska E, Wojciechowska C, Glanowska G, Wilczewski P, Niklewski T, Zembala M, Polonski L, Rozek MM, Wodniecki J (2001) Randomized, placebo-controlled study for immunosuppressive treatment of inflammatory dilated cardiomyopathy: two-year follow-up results. Circulation 104:39–45
47. Kwon HJ, Coté TR, Cuffe MS, Kramer JM, Braun MM (2003) Case reports of heart failure after therapy with a tumor necrosis factor antagonist. Ann Intern Med 138:807–811
48. Mann DL, Mcmurray JJ, Packer M, Swedberg K, Borer JS, Colucci WS, Djian J, Drexler H, Feldman A, Kober L, Krum H, Liu P, Nieminen M, Tavazzi L, Van Veldhuisen DJ, Waldenstrom A, Warren M, Westheim A, Zannad F, Fleming T (2004) Targeted anticytokine therapy in patients with chronic heart failure: results of the Randomized Etanercept Worldwide Evaluation (RENEWAL). Circulation 109:1594–1602
49. Chung ES, Packer M, Lo KH, Fasanmade AA, Willerson JT (2003) Randomized, double-blind, placebo-controlled, pilot trial of infliximab, a chimeric monoclonal antibody to tumor necrosis factor-alpha, in patients with moderate-to-severe heart failure: results of the anti-TNF Therapy Against Congestive Heart Failure (ATTACH) trial. Circulation 107:3133–3140
50. Wang J, Zhou H (2020) Mitochondrial quality control mechanisms as molecular targets in cardiac ischemia-reperfusion injury. Acta Pharm Sin B 10:1866–1879
51. Zhou H, Ren J, Toan S, Mui D (2021) Role of mitochondrial quality surveillance in myocardial infarction: from bench to bedside. Ageing Res Rev 66:101250
52. Picca A, Mankowski RT, Burman JL, Donisi L, Kim JS, Marzetti E, Leeuwenburgh C (2018) Mitochondrial quality control mechanisms as molecular targets in cardiac ageing. Nat Rev Cardiol 15:543–554
53. Ikeda Y, Shirakabe A, Maejima Y, Zhai P, Sciarretta S, Toli J, Nomura M, Mihara K, Egashira K, Ohishi M, Abdellatif M, Sadoshima J (2015) Endogenous Drp1 mediates mitochondrial autophagy and protects the heart against energy stress. Circ Res 116:264–278
54. Qiu Z, Wei Y, Song Q, Du B, Wang H, Chu Y, Hu Y (2019) The role of myocardial mitochondrial quality control in heart failure. Front Pharmacol 10:1404
55. Shirakabe A, Zhai P, Ikeda Y, Saito T, Maejima Y, Hsu CP, Nomura M, Egashira K, Levine B, Sadoshima J (2016) Drp1-dependent mitochondrial autophagy plays a protective role against pressure overload-induced mitochondrial dysfunction and heart failure. Circulation 133:1249–1263
56. Yu LM, Dong X, Xue XD, Xu S, Zhang X, Xu YL, Wang ZS, Wang Y, Gao H, Liang YX, Yang Y, Wang HS (2021) Melatonin attenuates diabetic cardiomyopathy and reduces myocardial vulnerability to ischemia-reperfusion injury by improving mitochondrial quality control: role of SIRT6. J Pineal Res 70:e12698
57. Viswanathan MC, Blice-Baum AC, Sang TK, Cammarato A (2016) Cardiac-restricted expression of VCP/TER94 RNAi or disease alleles perturbs drosophila heart structure and impairs function. J Cardiovasc Dev Dis 3:19
58. Yi P, Higa A, Taouji S, Bexiga MG, Marza E, Arma D, Castain C, Le Bail B, Simpson JC, Rosenbaum J, Balabaud C, Bioulac-Sage P, Blanc JF, Chevet E (2012) Sorafenib-mediated targeting of the AAA^+ ATPase p97/VCP leads to disruption of the secretory pathway, endoplasmic reticulum stress, and hepatocellular cancer cell death. Mol Cancer Ther 11:2610–2620
59. Zhu K, Cai Y, Si X, Ye Z, Gao Y, Liu C, Wang R, Ma Z, Zhu H, Zhang L, Li S, Zhang H, Yue J (2022) The phosphorylation and dephosphorylation switch of VCP/p97 regulates the architecture of centrosome and spindle. Cell Death Differ. https://doi.org/10.1038/s41418-022-01000-4
60. Zou R, Tao J, Qiu J, Lu H, Wu J, Zhu H, Li R, Mui D, Toan S, Chang X, Zhou H, Fan X (2022) DNA-PKcs promotes sepsis-induced multiple organ failure by triggering mitochondrial dysfunction. J Adv Res 41:39–48
61. Wang S, Zhu H, Li R, Mui D, Toan S, Chang X, Zhou H (2022) DNA-PKcs interacts with and phosphorylates Fis1 to induce mitochondrial fragmentation in tubular cells during acute kidney injury. Sci Signal 15:eabh1121
62. Silva JF, Olivon VC, Mestriner FLAC, Zanotto CZ, Ferreira RG, Ferreira NS, Silva CAA, Luiz JPM, Alves JV, Fazan R, Cunha FQ, Alves-Filho JC, Tostes RC (2020) Acute increase in O-GlcNAc improves survival in mice with LPS-induced systemic

inflammatory response syndrome. Front Physiol. https://doi.org/10.3389/fphys.2019.01614
63. Chu M, Qian L, Zhu M, Yao J, Xu D, Chen M (2018) Circumferential strain rate to detect lipopolysaccharide-induced cardiac dysfunction: a speckle tracking echocardiography study. Quant Imaging Med Surg 9:151–159
64. Elsawy H, Almalki M, Elmenshawy O, Abdel-Moneim A (2022) In vivo evaluation of the protective effects of arjunolic acid against lipopolysaccharide-induced septic myocardial injury. PeerJ 10:e12986
65. Sun Y, Yao X, Zhang QJ, Zhu M, Liu ZP, Ci B, Xie Y, Carlson D, Rothermel BA, Sun Y, Levine B, Hill JA, Wolf SE, Minei JP, Zang QS (2018) Beclin-1-dependent autophagy protects the heart during sepsis. Circulation 138:2247–2262
66. Zhou H, Toan S, Zhu P, Wang J, Ren J, Zhang Y (2020) DNA-PKcs promotes cardiac ischemia reperfusion injury through mitigating BI-1-governed mitochondrial homeostasis. Basic Res Cardiol 115:11
67. Zhou H, Zhu P, Wang J, Zhu H, Ren J, Chen Y (2018) Pathogenesis of cardiac ischemia reperfusion injury is associated with CK2alpha-disturbed mitochondrial homeostasis via suppression of FUNDC1-related mitophagy. Cell Death Differ 25:1080–1093
68. Guo W, Jiang L, Bhasin S, Khan SM, Swerdlow RH (2009) DNA extraction procedures meaningfully influence qPCR-based mtDNA copy number determination. Mitochondrion 9:261–265
69. Zhou H, Wang J, Zhu P, Zhu H, Toan S, Hu S, Ren J, Chen Y (2018) NR4A1 aggravates the cardiac microvascular ischemia reperfusion injury through suppressing FUNDC1-mediated mitophagy and promoting Mff-required mitochondrial fission by CK2alpha. Basic Res Cardiol 113:23